Time Reversal in Multiple-Input Multiple-Output Radar

Yuanwei Jin, *Senior Member, IEEE*, José M. F. Moura, *Fellow, IEEE*, and Nicholas O'Donoughue, *Student Member, IEEE*

***Abstract*—Time reversal explores the rich scattering in a multipath environment to achieve high target detectability. Multiple-input multiple-output (MIMO) radar is an emerging active sensing technology that uses diverse waveforms transmitted from widely spaced antennas to achieve increased target sensitivity when compared to standard phased arrays. In this paper, we combine MIMO radar with time reversal to automatically match waveforms to a scattering channel and further improve the performance of radar detection. We establish a radar target model in multipath rich environments and develop likelihood ratio tests for the proposed time-reversal MIMO radar (TR-MIMO). Numerical simulations demonstrate improved target detectability compared with the commonly used statistical MIMO strategy.**

***Index Terms*—Detection, multiple-input multiple-output (MIMO) radar, time reversal, waveform design.**

I. Introduction

MULTIPATH is a common phenomenon in radar, sonar, and wireless communication applications [1]–[3]. Most radar systems are designed under line-of-sight (LOS), not in multipath rich environments. Multipath has noticeable impact on radar performance. For example, the range of radar sensors is limited by LOS blockage due to buildings, forests, and many other scatterers. Hence, radar sensors usually attempt to maintain a very high aspect angle to avoid shadows in urban environments or forest areas, which severely reduces the coverage area. Multipath may also reduce the radar resolution and sensitivity to detecting targets. The multipath limitation has motivated extensive research on radar algorithm and architecture design to overcome the LOS restriction. In this paper, rather than treating multipath as an adverse effect, we use time reversal to explore multipath to enhance radar detection.

Manuscript received February 03, 2009; revised July 06, 2009. Current version published January 20, 2010. This work is supported in part by the Department of Energy under Award DE-NT-0004654, the National Science Foundation under Award CNS-093-868, and the Defence Advanced Research Projects Agency through the Army Research Office under Grant W911NF-04-1-0031. The work of N. O'Donoughue was supported by a National Defense Science and Engineering Graduate (NDSEG) Fellowship. The associate editor coordinating the review of this manuscript and approving it for publication was Dr. Michael Wicks.

Y. Jin is with Department of Engineering and Aviation Sciences, University of Maryland Eastern Shore, Princess Anne, MD 21853 USA (e-mail: yjin@umes.edu).

J. M. F. Moura and N. O'Donoughue are with Department of Electrical and Computer Engineering, Carnegie Mellon University, Pittsburgh, PA 15213 USA (e-mail: moura@ece.cmu.edu; nodonoug@ece.cmu.edu).

Color versions of one or more of the figures in this paper are available online at http://ieeexplore.ieee.org.

Digital Object Identifier 10.1109/JSTSP.2009.2038983

In time reversal (phase conjugation in the frequency domain), a short pulse, for example, transmitted by a source through a dispersive medium, is received by an array, then time reversed, energy normalized, and retransmitted through the same medium. If the scattering channel is reciprocal and sufficiently rich, the retransmitted waveform refocuses on the original source. By time reversal, the transmission waveforms are tailored to the propagation medium and the target scattering characteristics. Hence, time reversal is a radar waveform adaptive transmission scheme. Other radar waveform design strategies are given in, e.g., [4]–[6]. Our recent work, [7]–[9] considers signal detection using time reversal with a single antenna pair as well as with antenna arrays, and demonstrates that the time reversal generalized likelihood ratio detector (TR-GLRT) significantly improves detection performance when compared with conventional detectors.

Recently, there has been considerable interest in a novel class of radar systems known as "MIMO radar," where the term multiple-input multiple-output (MIMO) refers to the use of multiple-transmit as well as multiple-receive antennas [10]–[15]. Most authors assume that the key aspect of a MIMO radar system is the use of a set of orthogonal transmit waveforms. The radar return from a given scatterer has various degrees of correlation across the array, depending on the element spacing and array configuration. In particular, the term "statistical MIMO radar," [10], refers to the signal model where the signals measured at different antennas are uncorrelated. If the antennas are separated far enough, the target radar cross sections (RCS) for different transmitting paths become independent random variables. Thus, each orthogonal waveform carries independent information about the target; spatial diversity about the target is thus created. Exploiting the independence between signals at the array elements, MIMO radar achieves improved detection performance and increased radar sensitivity. This is in contrast with a conventional phased array that presupposes a high correlation between signals either transmitted or received by an array.

In this paper, we develop a MIMO setup to operate in a rich scattering environment and to exploit the multipath propagation. There are many mechanisms that cause multipath in radar detection, for example, the presence of a large number of scatterers in the vicinity of the target of interest, or tracking and detection of low-angle targets over a flat surface [16], [17]. Multipath affects the level of the energy return from the target due to coherent combining of the return signals. As a result, we will observe fades and enhancements relative to the level that is expected in a free-space environment. In general, the overall target response is characterized by the target's radar cross section, the multipath

propagation due to the surrounding scatterers, and the antenna's aspect angle. The unknown nature of the complex target reflection makes the overall target response appear to be *random* even for a *point target*. Therefore, we adopt a statistical model for the target in this paper. Although our MIMO model is somehow similar to what is used in [10], the difference is clear. In [10], the randomness of the radar target return is caused by many look angles from *extended* targets; in our case, the randomness of a (point) target response is the result of multipath.

In this paper, we combine time reversal with MIMO (TR-MIMO) radar technology to improve the signal-to-noise ratio by tailoring the transmitted waveforms to the propagation medium and the target scattering characteristics. The benefits of the proposed TR-MIMO detection include: 1) to exploit the spatial diversity arising from the multipath propagation; 2) to use time reversal to adaptively adjust the radar waveforms to scattering characteristics of the channel; 3) to employ simple orthogonal wideband waveforms without seeking complicated waveform coding design methods; and 4) to incorporate the de-correlation between the forward channel and the backward channel when the reciprocity condition may not strictly hold. We develop a binary hypothesis detector for the TR-MIMO and provide analytical expressions for the test statistic. In previous work [7]–[9], [18], [19], we showed that time reversal offered higher resolution and improved detectability over conventional methods. In this paper, we demonstrate that a MIMO radar combined with time reversal (TR-MIMO) improves target detectability when compared with statistical MIMO (S-MIMO) [20].

The remainder of the paper is organized as follows. Section II discusses the MIMO modeling in multipath. Section III discusses the TR-MIMO signal modeling. Section IV derives the TR-MIMO detectors. Section V provides performance analysis for the proposed MIMO detector. Section VI presents the TR-MIMO detection results. Finally, conclusions are drawn in Section VII.

II. MIMO Modeling in Multipath

We consider the problem of detecting a stationary or slowly moving target immersed in a multipath rich scattering environment. Such scenarios occur in many radar applications, for example, detection through tree canopy or low-angle detection and tracking. In this section, we derive the MIMO radar model.

A. Overview of Statistical MIMO Radar Modeling

In statistical MIMO radar [20], antennas at the transmitter and the receiver of the radar are well separated such that they experience an angular spread caused by variation of the radar cross section (RCS). Statistical MIMO radar utilizes the *spatial diversity* introduced by the radar target fluctuation. For extended targets, due to the large inter-element spacing between the antennas, each transmitter–receiver pair sees a different aspect of the target. This observation yields the following basic MIMO radar modeling for extended targets [20]:

$$\mathbf{r}(t) = \sqrt{\frac{E}{M}}\mathbf{H}\mathbf{s}(t-\tau) + \mathbf{n}(t) \tag{1}$$

where $\mathbf{H}$ is an $N \times M$ matrix, referred to as the target channel matrix, and

$$[\mathbf{H}]_{i,m} = h_{i,m},\ i = 1, \cdots, N, m = 1, \cdots, M. \tag{2}$$

The $h_{i,m}$ are independent complex normal random variables. The vector $\mathbf{r}(t) = [r_1(t), \cdots, r_N(t)]^T$ is the collection of received signals at the receive antennas. The vector $\mathbf{s}(t) = [s_1(t), \cdots, s_M(t)]^T$ is the collection of the transmit signals at the transmit antennas. The vector $\mathbf{n}(t)$ is the additive noise. Given the statistical MIMO model (1), the optimal detector is a non-coherent detector given by [20]

$$\ell(\mathbf{r}) = \sum_{i=1}^{N}\sum_{m=1}^{M}\left|\int r_i(t)s_m(t-\tau)dt\right|^2. \tag{3}$$

Remarks:

1) The radar model (2) is justified in that the received echoes from an *extended target* between each pair of transmit antenna and receive antenna become independent random variables when the antennas are placed sparsely. We will show that multipath causes a similar effect even when the target is pointwise. The superposition of the multipath adding constructively and destructively makes the received radar returns appear to be random.
2) This observation can be further justified by examining the radar operating spectrum for a point target. A point target in a LOS condition yields a flat spectrum for the returned signal, but results in a fluctuating spectrum in a non-LOS condition.
3) The radar model (2) and the processing (3) are designed for narrowband systems. By exploring the orthogonality of the waveforms, each receiver may match to a specified transmit waveform [20]. To extend this design scheme to a wideband system is difficult and may significantly increase the radar system complexity. This is because of the difficulty in designing orthogonal radar waveforms that can meet various radar operational conditions (e.g., [21]). On the other hand, (3) indicates that the signal cross-correlation can not be disregarded; significant correlation reduces the mainlobe width, which can result into higher ambiguity sidelobe levels. This paper proposes a simple quasi-orthogonal waveform design for wideband MIMO radar using the time reversal method.

Next, we introduce a point target MIMO model in multipath environments.

B. Multipath MIMO Radar Model

In the absence of multipath, the reflected radar waveform from a point target is an amplitude scaled and time delayed replica of the transmitted waveform. In theory, the target frequency response is flat. However, multipath propagation induces a rapid fluctuation in the frequency response of the point target. Fig. 1 illustrates a two-way radar propagation model in multipath. For simplicity, this model considers a two-path propagation with only a single reflected ray emanating from a virtual target image. The two-path propagation is caused by scatterers between the receiving array B and the target. This model can be extended to the more general scenario with

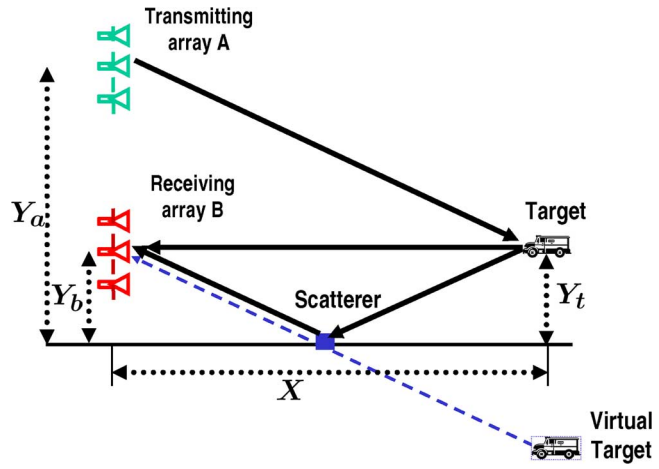

Fig. 1. Multipath propagation model. Only the forward propagation (from array A to array B) is illustrated.

multiple path propagation due to scatterers in the fields of view of both the transmitting array A and receiving array B.

Suppose we have a transmitting signal

$$s_{\mathrm{Tx},m}(f) = S_m(f)e^{j2\pi f_c t} \tag{4}$$

where $S_m(f)$ is the baseband radar pulse at frequency f from the mth transmit antenna, f_c is the carrier frequency. We assume that the signal propagates in the multipath medium and reflects from a target with a possible phase change θ. The noise-free received signal at the ith element of array B due to the mth transmit antenna at array A is given by

$$s_{\mathrm{Rx},i}(f) = \xi_{im}\left(e^{j(2\pi f_c t-\theta_{im}-2\pi f_c\tau_{0,im})} + A_{1,im}e^{j(2\pi f_c t-\theta_{1,im}-2\pi f_c\tau_{1,im})}\right) \tag{5}$$

where $\theta_{1,im}$ is the phase change due to the multipath; the direct path delay $\tau_{0,im}$ and the multipath delay $\tau_{1,im}$ are given as follows:

$$\tau_{0,im} = \frac{\sqrt{X^2+(Y_a-Y_t)^2}+\sqrt{X^2+(Y_b-Y_t)^2}}{c} \tag{6}$$

$$\tau_{1,im} = \frac{\sqrt{X^2+(Y_a-Y_t)^2}+\sqrt{X^2+(Y_b+Y_t)^2}}{c} \tag{7}$$

The symbols Y_a, Y_b, and Y_t are the azimuth coordinates of the mth antenna at A, the ith antenna at B, and the target, respectively; X is the target range; and ξ_{im} is the complex amplitude due to the target characteristics. The complex amplitudes of the direct and reflected rays are simply related by a complex multipath reflection coefficient $A_{1,im}$.

By mixing the received signal with the transmitted signal, we obtain the baseband signal as follows:

$$s_{\mathrm{B},i}(f) = \xi_{im}\left(e^{-j(\theta_{im}+2\pi f_c\tau_{0,im})} + A_{1,im}e^{-j(\theta_{1,im}+2\pi f_c\tau_{1,im})}\right)|S_m(f)|^2 \tag{8}$$

With a large number of scatterers L and $A_{l,im}$, $l=0,\cdots,L-1$, multipath reflection coefficients, we obtain the overall target reflectivity

$$\begin{aligned} s_{\mathrm{B},m}(f) &= \xi_{im}\sum_{l=0}^{L-1} A_{l,im}e^{-j[\theta_{l,im}+2\pi f_c\tau_{l,im}]}\,|S_m(f)|^2 \\ &= h_{im}(f)\,|S_m(f)|^2 \end{aligned} \tag{9}$$

where the target channel response between the ith antenna in array B and the mth antenna in array A is

$$h_{im}(f) = \xi_{im}\sum_{l=0}^{L-1} A_{l,im}e^{-j[\theta_{l,im}+2\pi f_c\tau_{l,im}]}. \tag{10}$$

We hence assume that, with a large number of scatterers L and multipath reflection coefficients $A_{l,im}$, the overall target reflectivity (10) is a *random* variable. This analysis implies that, even for a point target, the multipath effect induces fades and enhancements in the returned signals relative to the free space returned signals. The transmit and receive antenna pairs provide independent information about the target due to their different viewing angles.

Hence, from (10), we introduce the **forward propagation channel**. We let $\mathbf{H}(f)$ denote the forward channel response matrix between the transmit array A and the receive array B at frequency f. The (i,m)th entry of $\mathbf{H}(f)$, i.e., the forward channel response from antenna A_m, $m=1,\cdots,M$, to antenna B_i, $i=1,\cdots,N$, is

$$[\mathbf{H}(f)]_{i,m} = h_{im}(f) \sim \mathcal{CN}\left(0,\sigma_s^2(f)\right) \tag{11}$$

where the symbol $\sim$ stands for "distributed as." The target channel model (11) implies that, at a fixed frequency f and for each transmitter antenna and receiver antenna pair, the target channel response is a complex Gaussian random variable with zero mean and variance $\sigma_s^2(f)$. This variance (i.e., the power spectrum density) is frequency dependent, which is caused by the multipath scattering. Further, we assume that the channel response from different transmit and receive pairs are statistically independent, identically distributed (i.i.d.) random variables. Note that the frequency-domain representation $h_{im}(f)$ is related to the time-domain channel impulse response $h_{im}(t)$,

$$h_{im}(f) = \frac{1}{T}\int_0^T h_{im}(t)e^{-j2\pi ft}dt \tag{12}$$

where the RCS of the target $h_{im}(t)$ is modeled as a zero mean, finite covariance, wide sense stationary uncorrelated scattering (WSSUS) Gaussian process. This assumption is valid for many practical situations in wave propagation in the radar literature [22], [23]. The variance $\sigma_s^2(f)$ of $h_{im}(f)$ is frequency dependent. By the WSSUS assumption and the Wiener–Khintchine theorem [24]

$$\lim_{T\to\infty}\frac{1}{T}E\left\{|h_{im}(f)|^2\right\} = K_h(f) \tag{13}$$

where $K_h(f)$ is the power spectral density (PSD) of $h_{im}(t)$, i.e., the Fourier transform of the covariance function

$$\kappa_h(\tau) = E\{h_{im}(t)h_{im}(t+\tau)\} \tag{14}$$

$$K_h(f) = \int_{-\infty}^{\infty} \kappa_h(\tau) e^{-j2\pi f\tau} d\tau. \tag{15}$$

Hence, by (13)

$$\sigma_s^2(f) \approx T \cdot K_h(f) \tag{16}$$

In general, pulse wave propagation and scattering in a random medium can be characterized by the correlation function (see chapter §5 in [22])

$$\Gamma(f, f+\Delta f, t', t'+\Delta t') = \frac{E\{h_{im}(f,t')h_{im}^*(f+\Delta f, t'+\Delta t')\}}{\sigma_s^2(f,t')} \tag{17}$$

The function $\Gamma(\cdot)$ is the correlation function between the output fields due to the time-harmonic inputs at two different frequencies f and $f+\Delta f$. We should note that the time-varying frequency response of the random channel $h_{im}(f,t')$ in (17) shows explicitly the time index t' that is omitted in (12). If we let $\Delta t' = 0$ and send two waves at different frequencies f and $f+\Delta f$, and observe the fluctuation fields at the same time, as we separate the frequencies, the correlation of these two fluctuation fields decreases. For uncorrelated scattering channel, the function $\Gamma(f, f+\Delta f, t', t')$ is a function of the frequency separation Δf.

In a multipath channel, it is often convenient to consider the coherence bandwidth B_c measured by the reciprocal of the *multipath spread*. Two sinusoids with frequency separation greater than B_c are affected quite differently by the channel. Hence, the frequency samples taken $\Delta f = B_c$ apart are considered to be, approximately, independent. Therefore, we use discrete frequency samples f_q, $q = 0, \cdots, Q-1$, in developing the TR-MIMO detector. The number Q is chosen by

$$Q = \frac{B}{B_c} \tag{18}$$

where B_c is the coherence bandwidth of the multipath channel, and B is the system bandwidth. The richer the multipath scattering, the smaller the coherence bandwidth, and so the larger the quantity Q.

C. Wideband Orthogonal Waveform Signaling

MIMO radar typically transmits a set of orthogonal waveforms from different antennas. In our problem, the simultaneously transmitted waveforms occupy the same frequency range. We let the transmitting signal from the mth antenna be

$$s_m(t) = s\left(t - \frac{m}{B}\right). \tag{19}$$

To achieve the orthogonality among the transmitted waveforms, we assume that

$$\int_0^T s_m(t)s_l^*(t)dt = \int_0^T s\left(t-\frac{m}{B}\right)s^*\left(t-\frac{l}{B}\right)dt \approx 0, \ \ l \neq m \tag{20}$$

This assumption is accurate for linear frequency modulated (LFM) signals and provides a good approximation for other wideband signals such hyperbolic frequency modulation (HFM) signals, as well as signals generated from pseudo random sequences [23]. Using the orthogonality condition in (20), and converting it into the frequency domain by the Fourier transform, we get

$$\begin{aligned}
&\frac{1}{T}\int_0^T s\left(t-\frac{m}{B}\right)s^*\left(t-\frac{l}{B}\right)dt \\
&\quad = \int_{-\infty}^{\infty}\int_{-\infty}^{\infty} S(f)S^*(f')e^{j2\pi f\frac{m}{B} - j2\pi f'\frac{l}{B}} \\
&\qquad \times \frac{1}{T}\int_0^T e^{j2\pi(f-f')t}dt\,df\,df' \qquad (21)\\
&\quad = \int_{-\infty}^{\infty}\int_{-\infty}^{\infty} S(f)S^*(f')e^{j2\pi f\frac{m}{B} - j2\pi f'\frac{l}{B}} \\
&\qquad \cdot \operatorname{sinc}\left((f-f')T\right)df\,df' \qquad (22)\\
&\quad \approx \int_{-\infty}^{\infty} |S(f)|^2 e^{j2\pi f\frac{m-l}{B}}df \\
&\quad = \delta(m-l) \qquad (23)
\end{aligned}$$

where $\operatorname{sinc}(x) = \sin(x)/x$, and we assume that $|S(f)|^2 = 1$. Using discrete frequency samples, for $f_q = q\Delta f$, $\Delta f = B/Q$, and $q = 0, \cdots, Q-1$, we obtain a phase coding scheme, [25], by setting

$$S_m(f_q) = e^{j2\pi\frac{mq}{Q}}S(f_q), \ \ q = 0, 1, \cdots, Q-1 \tag{24}$$

for $m = 1, \cdots, M \leq Q$. For transmit antennas m and l, it is straightforward to show that

$$\sum_{q=0}^{Q-1} S_m(f_q)S_l^*(f_q) = Q\delta(m-l). \tag{25}$$

III. Time Reversal MIMO Signal Model

In this section, we describe the time reversal MIMO radar signal model. In time reversal, the received signal is phase conjugated, energy normalized, and retransmitted to the same medium. If the medium is reciprocal, the forward propagation channel is the same as the backward propagation channel. However, in many radar applications, the reciprocity condition may not hold, for example, due to small random perturbations between the forward and the backward channel realizations, or due to slow target motion. Hence, we model the backward propagation channel as follows with respect to the forward

channel given in (11): let $[\overline{\mathbf{H}}(f_q)]^T$ denote the backward channel frequency response matrix between the array A and B. The symbol $(\cdot)^T$ denotes the transpose. The propagation channel from antenna B_i, $i = 1,\cdots,N$, to antenna A_m, $m = 1,\cdots,M$, is given by

$$\left[\left(\overline{\mathbf{H}}(f_q)\right)^T\right]_{i,m} \triangleq \bar{h}_{im}(f_q) = \rho \cdot h_{im}(f_q) + \gamma_{im}(f_q) \quad (26)$$

where (26) models the backward channel as a noisy version of the forward channel: the symbol ρ is the correlation coefficient between the forward channel $h_{im}(f_q)$ and the backward channel $\bar{h}_{im}(f_q)$. The term $\gamma_{im}(f_q)$ describes the channel disturbance that occurs between the forward and backward channel for each pair of transmit and receive antennas in A and B. We assume that the disturbance is independent of $h_{im}(f_q)$; it is distributed as a complex Gaussian with zero mean and variance $\sigma_\gamma^2(f_q)$, i.e., $\gamma_{im}(f_q) \sim \mathcal{CN}(0, \sigma_\gamma^2(f_q))$. We further impose the constraint that $\bar{h}_{im}(f_q)$ has the same variance $\sigma_s^2(f_q)$ as $h_{im}(f_q)$, i.e.,

$$\bar{h}_{im}(f_q) \sim \mathcal{CN}\left(0, \sigma_s^2(f_q)\right) \quad (27)$$

which implies that

$$\rho = \sqrt{1 - \frac{\sigma_\gamma^2(f_q)}{\sigma_s^2(f_q)}} \leq 1. \quad (28)$$

When $\rho < 1$, the quantity ρ captures the de-correlation between the forward channel and the backward channel. As discussed above, the de-correlation can happen due to slow changes on the media [26], [27]; its net effect is to degrade the reciprocity condition. The characterization of the degradation is important to analyze the performance of time reversal MIMO radar. Let

$$\left[\left(\mathbf{\Gamma}(f_q)\right)^T\right]_{i,m} \triangleq \gamma_{im}(f_q). \quad (29)$$

Equation (26) can then be rewritten in matrix form as

$$\left[\overline{\mathbf{H}}(f_q)\right]^T = \rho\left[\mathbf{H}(f_q)\right]^T + \left[\mathbf{\Gamma}(f_q)\right]^T. \quad (30)$$

A. TR-MIMO Data Collection and Processing

The time reversal radar data collection and processing are described in three steps as follows.

Step 1 Target Probing: The signal vector received at array B for the lth data snapshot is

$$\mathbf{y}_l(f_q) = \mathbf{p}(f_q) + \mathbf{w}_l(f_q). \quad (31)$$

where

$$\mathbf{p}(f_q) = \mathbf{H}(f_q)\mathbf{s}_A(f_q). \quad (32)$$

is a $N \times 1$ vector. The $M \times 1$ signal vector $\mathbf{s}_A(f_q)$ transmitted from array A is

$$\mathbf{s}_A(f_q) = [S_1(f_q),\cdots,S_M(f_q)]^T, \quad q = 0,\cdots,Q-1. \quad (33)$$

The transmitted signal $s_i(t)$ from the ith antenna is a wideband signal with Fourier representation $S_i(f_q)$ at frequency f_q. We assume that the average transmission power at each antenna is the same

$$E_s = \frac{1}{Q}\sum_{q=0}^{Q-1}\left|S_i(f_q)\right|^2. \quad (34)$$

In this step, the total transmission energy is ME_s. The noise vector $\mathbf{w}_l(f_q)$ is characterized statistically as

$$\mathbf{w}_l(f_q) \sim \mathcal{CN}\left(0, \sigma_n^2\mathbf{I}\right),\ l = 1,\cdots,L. \quad (35)$$

We assume here that the clutter is homogeneous; the noise vector (35) describes both the homogeneous clutter and the additive noise in the received radar returns. We should note that this is a very simplified assumption on the clutter. Statistical models for MIMO radar clutter should incorporate a number of effects including geometry, coherence, transmit waveform, multipath scattering, etc. Development of statistical models for MIMO radar clutter is beyond the scope of this paper. In general, inhomogeneous clutter can be suppressed using whitening filters in the spectral and spatial subspaces (see, e.g., [28] and [29]). Next, suppose we can collect $l = 0,\cdots,L-1$ snapshots, for a slow varying target channel. The minimum mean squared estimate of the returned target signal is

$$\widehat{\mathbf{p}}(f_q) = \mathbf{p}(f_q) + \overline{\mathbf{w}}(f_q) \quad (36)$$

where $\overline{\mathbf{w}}(f_q) = (1/L)\sum_{l=0}^{L-1}\mathbf{w}_l(f_q)$. We assume that we can obtain a reasonably accurate estimate of the target channel response for sufficiently large L. In the subsequent derivation, we assume that we know $\mathbf{p}(f_q)$ precisely. This assumption yields the ideal scenario for the TR-MIMO detector. In reality, we would use $\widehat{\mathbf{p}}(f_q)$ as the signal to be retransmitted. The problem of obtaining a sufficient number of snapshots L for this purpose is governed by two important factors: 1) the scale over which the response changes with respect to space and time; and 2) systems considerations such as the bandwidth that limit the sampling rate. Thus, in a radar setting it is fairly common to have a snapshot starved scenario. In this case, the noise variance will increase. Our early attempts to analyzing the effect of noise variance increase have been reported in [8]. The detection performance under this scenario will be studied below by simulations. We note that a larger L means longer estimation time that yields target channel partial de-correlation in time reversal.

Step 2: Time Reversal Probing: Conventional detection processes the data received at array B. With time reversal, the received radar return at array B is transmitted back to array A. Prior to retransmission, the data vector $\mathbf{p}(f_q)$ is time reversed and energy normalized. The $M \times 1$ received signal vector at array A is

$$\begin{aligned}
\mathbf{x}_l(f_q) &\triangleq [X_{l,1}(f_q),\cdots,X_{l,M}(f_q)]^T && (37)\\
&= \underbrace{\overline{\mathbf{H}}^T(f_q)\left[k\mathbf{p}(f_q)\right]^*}_{\text{target return } \mathbf{c}(f_q)} + \mathbf{v}_l(f_q) && (38)\\
&= k\overline{\mathbf{H}}^T(f_q)\mathbf{H}^*(f_q)\mathbf{s}_A^*(f_q) + \mathbf{v}_l(f_q) && (39)\\
&= k\rho\mathbf{H}^T(f_q)\mathbf{H}^*(f_q)\mathbf{s}_A^*(f_q)\\
&\quad + k\mathbf{\Gamma}^T(f_q)\mathbf{H}^*(f_q)\mathbf{s}_A^*(f_q) + \mathbf{v}_l(f_q) && (40)
\end{aligned}$$

where the scalar k is the energy normalization factor

$$k = \sqrt{\frac{QME_s}{\sum_{q=0}^{Q-1}\left\|\mathbf{p}(f_q)\right\|^2}}. \quad (41)$$

This factor normalizes the energy of the time reversed retransmitted signal to equal the energy of the original transmitted signal $\mathbf{s}_A(t)$. The target return is defined as

$$\mathbf{c}(f_q) = \overline{\mathbf{H}}^T(f_q)\left[k\mathbf{p}(f_q)\right]^* = [C_1(f_q),\cdots,C_M(f_q)]^T. \quad (42)$$

The noise vector, defined by

$$\mathbf{v}_l(f_q) = [V_{l,1}(f_q), \cdots, V_{l,M}(f_q)]^T \tag{43}$$

is distributed as $\mathbf{v}_l(f_q) \sim \mathcal{CN}(0, \sigma_n^2 \mathbf{I})$. We use $\overline{\mathbf{H}}^T(f_q)$ in (26) rather than $\mathbf{H}(f_q)$ to account for the backward channel de-correlation due to the changes on the propagation media.

Step 3: Signal Matched Filtering: The received signal $\mathbf{x}_l(f_q)$, $q = 0, \cdots, Q-1$ in (38) is a $M \times 1$ vector. The ith entry of $\mathbf{x}_l(f_q)$, $X_{l,i}$ defined in (37), is the received radar return at the ith antenna of array A. This radar signal will be matched with the originally transmitted signal at the ith antenna, i.e., $S_i(f_q)$ defined in (33).[1] We repeat this process for $i = 1, \cdots M$ antennas at the array A, which yields the following $M \times 1$ data vector

$$\mathbf{r}_l \triangleq [R_{l,1}, \cdots, R_{l,M}]^T \tag{44}$$

$$= \sum_{q=0}^{Q-1} \operatorname{diag}[\mathbf{s}_A(f_q)]\, \mathbf{x}_l(f_q) \tag{45}$$

$$= \begin{bmatrix} \sum_{q=0}^{Q-1} X_{l,1}(f_q) S_1(f_q) \\ \sum_{q=0}^{Q-1} X_{l,2}(f_q) S_2(f_q) \\ \vdots \\ \sum_{q=0}^{Q-1} X_{l,M}(f_q) S_M(f_q) \end{bmatrix} \tag{46}$$

$$= \begin{bmatrix} \sum_{q=0}^{Q-1} C_1(f_q) S_1(f_q) + \sum_{q=0}^{Q-1} V_{l,1}(f_q) S_1(f_q) \\ \sum_{q=0}^{Q-1} C_2(f_q) S_2(f_q) + \sum_{q=0}^{Q-1} V_{l,2}(f_q) S_2(f_q) \\ \vdots \\ \sum_{q=0}^{Q-1} C_M(f_q) S_M(f_q) + \sum_{q=0}^{Q-1} V_{l,M}(f_q) S_M(f_q) \end{bmatrix} \tag{47}$$

where in (47) C_i and $V_{l,i}$, $i = 1, \cdots, M$, are defined in (42) and (43), respectively. Hence, we can rewrite (45) in vector form as

$$\mathbf{r}_l = \widetilde{\mathbf{c}} + \widetilde{\mathbf{v}}_l \tag{48}$$

where

$$\widetilde{\mathbf{c}} = [\widetilde{C}_1, \cdots, \widetilde{C}_M]^T, \;\; \widetilde{C}_i = \sum_{q=0}^{Q-1} C_i(f_q) S_i(f_q) \tag{49}$$

$$\widetilde{\mathbf{v}}_l = [\widetilde{V}_{l,1}, \cdots, \widetilde{V}_{l,M}]^T, \;\; \widetilde{V}_i = \sum_{q=0}^{Q-1} V_{l,i}(f_q) S_i(f_q). \tag{50}$$

IV. MIMO Detectors

In this section, we formulate the MIMO radar detection problem. The binary hypothesis test for TR-MIMO is

$$\begin{aligned} \mathbb{H}_1 &: \; \mathbf{r}_l = \widetilde{\mathbf{c}} + \widetilde{\mathbf{v}}_l \\ \mathbb{H}_0 &: \; \mathbf{r}_l = \widetilde{\mathbf{v}}_l. \end{aligned} \tag{51}$$

[1]One may argue that the received radar signal at the ith antenna, $X_{l,i}$, can be matched with the individual waveforms $S_1(f_q), \cdots, S_M(f_q)$. We show in Section IV that the output of the matched filter of $X_{l,i}$ with $S_j(f_q)$, $j \neq i$ is relatively small and then can be ignored.

The optimal detector, in the Neyman–Pearson sense, is the likelihood ratio test (LRT), i.e.,

$$\ell = \log \frac{f(\mathbf{r}_l|\mathbb{H}_1)}{f(\mathbf{r}_l|\mathbb{H}_0)} \underset{\mathbb{H}_0}{\overset{\mathbb{H}_1}{\gtrless}} \eta \tag{52}$$

where η is the decision threshold. The function $f(\mathbf{r}|\mathbb{H}_i)$, $i = 0, 1$, are the probability density functions of the received signal under $\mathbb{H}_0$ and $\mathbb{H}_1$, respectively. The detection problem (51) is a common problem: detecting a nonwhite Gaussian process immersed in additive nonwhite (or white) Gaussian noise in sonar or radar (see, e.g., [28]–[31]). A closed form for the probability density function for the binary hypothesis (51) is often difficult to obtain. Thus, we will rely on approximations and on the central limit theorem to study the data statistics and to derive the test statistics.

A. Data Statistics

By (49), the ith entry of $\widetilde{\mathbf{c}}$ is

$$\widetilde{C}_i = k \sum_{q=0}^{Q-1} \sum_{n=1}^{N} \bar{h}_{ni}(f_q) h_{ni}^*(f_q) \, |S_i(f_q)|^2 + k \sum_{q=0}^{Q-1} \underbrace{\sum_{j=1, j\neq i}^{N} \left(\sum_{n=1}^{N} \bar{h}_{ni}(f_q) h_{nj}^*(f_q) \right)}_{N(N-1) \text{ terms}} S_j^*(f_q) S_i(f_q). \tag{53}$$

Note that, the sum of the $N(N-1)$ terms in (53) can be approximated by

$$\begin{aligned} &\sum_{j=1, j\neq i}^{N} \left(\sum_{n=1}^{N} \bar{h}_{ni}(f_q) h_{nj}^*(f_q) \right) \\ &\quad \approx N(N-1) E\left(\bar{h}_{ni}(f_q) h_{nj}^*(f_q) \right) \\ &\quad = N(N-1) E\left(\bar{h}_{ni}(f_q) \right) E\left(h_{nj}^*(f_q) \right) \\ &\quad = 0 \end{aligned} \tag{54}$$

where $\bar{h}_{ni}(f_q)$ and $h_{nj}(f_q)$ are independent Gaussian random variables for $j \neq i$. Equation (54) greatly simplifies (53), which yields

$$\widetilde{C}_i \approx k \sum_{q=0}^{Q-1} \sum_{n=1}^{N} \bar{h}_{ni}(f_q) h_{ni}^*(f_q) \tag{55}$$

$$= k\rho \cdot \underbrace{\sum_{q=0}^{Q-1} \sum_{n=1}^{N} |h_{ni}(f_q)|^2}_{\text{focused target response}} + k \underbrace{\sum_{q=0}^{Q-1} \sum_{n=1}^{N} \gamma_{ni}(f_q) h_{ni}^*(f_q)}_{\text{perturbation term}} \tag{56}$$

where $|S_i(f_q)|^2 = 1$ by (24). However, by eliminating the unmatched phase terms in the analysis, (54) may introduce a small

prediction error compared with the results from numerical simulation. We will show by Monte Carol simulation in Section VI that this prediction error is within a fraction of a dB.

Next, we use χ^2_M to represent the central Chi-squared distribution with M degrees of freedom. Therefore, [32]

$$|h_{ni}(f_q)|^2 \sim \frac{\sigma_s^2(f_q)}{2}\chi_2^2 \tag{57}$$

which leads to $E\{|h_{ni}(f_q)|^2\} = \sigma_s^2(f_q)$, a frequency-dependent real constant. Hence, we can further approximate (56) as

$$E\{\widetilde{C}_i\} = \rho \cdot N \cdot E\{k\} \cdot \sum_{q=0}^{Q-1} \sigma_s^2(f_q). \tag{58}$$

Equations (56) and (58) show that the diagonal components $\widetilde{C}_i$ are the **focused** target response; in a statistical sense, by averaging out the perturbation term in (56), they are zero-phase quantities. This observation leads to the following approximation:

$$\widetilde{C}_i \approx \rho \cdot \sum_{q=0}^{Q-1} k \sum_{n=1}^{N} |h_{ni}(f_q)|^2 \tag{59}$$

By ignoring the perturbation term, we should note that, when the forward channel and backward channel are fully correlated, i.e., $\rho = 1$, the above approximation is exact. We will develop the TR-MIMO detector under this assumption. We will test for cases when $\rho < 1$ using numerical simulations. Let's further define

$$Z_i(f_q) \triangleq k \sum_{n=1}^{N} |h_{ni}(f_q)|^2 \simeq \overline{k}\frac{\sigma_s^2(f_q)}{2}\chi^2_{2N} \tag{60}$$

where, the symbol $\sim$ stands for "distributed as" and $\simeq$ stands for "distributed approximately as." The symbol $\overline{k} \triangleq E\{k\} \approx \sqrt{E\{k^2\}}$. For the sake of simplicity, here we treat k and $\sum_{n=1}^{N} |h_{ni}(f_q)|^2$ as two independent random variables. We further approximate k by the constant $E\{k\}$. We show in (129) and (133) in Appendix I that this is a valid approximation: the random variable k^2 is a low variance distribution with a constant mean. Next, we rewrite (59) as

$$\widetilde{C}_i = \rho \cdot \sum_{q=0}^{Q-1} Z_i(f_q). \tag{61}$$

The sequence $\{Z_i(f_q), \forall q\}$ are independent random variables with finite variance. By the Lindeberg–Lyapunov central limit theorem on sums of independent random variables [32],[2] the sequence $\{\widetilde{C}_i\}$ is asymptotically Gaussian for large Q. Hence, (61) yields

$$\widetilde{C}_i \simeq \mathcal{N}\left(\rho \cdot \sum_{q=0}^{Q-1} \mu(f_q), \rho^2 \cdot \sum_{q=0}^{Q-1} \Phi(f_q)\right) \tag{62}$$

[2]The Lindeberg–Lyapunov central limit theorem [33] generalizes the classical central limit theorem [34] by removing the identically distributed condition.

where

$$\mu(f_q) = E\{Z_i(f_q)\} = \overline{k}N\sigma_s^2(f_q), \tag{63}$$

$$\Phi(f_q) = Var\{Z_i(f_q)\} = \overline{k}^2 N\sigma_s^4(f_q). \tag{64}$$

B. TR-MIMO Detector

Hence, under $\mathbb{H}_1$ in the binary hypothesis (51), the ith entry of signal $\mathbf{r}_l$ becomes

$$R_{l,i} = \widetilde{C}_i + \widetilde{V}_i \tag{65}$$

$$= \widetilde{C}_i + \Re(\widetilde{V}_i) + \sqrt{-1} \cdot \Im(\widetilde{V}_i). \tag{66}$$

The symbols $\Re(x)$ and $\Im(x)$ denote the real and imaginary part of the complex number x. Both quantities $\widetilde{C}_i + \Re(\widetilde{V}_i)$ and $\Im(\widetilde{V}_i)$ are real numbers. Further notice that

$$\widetilde{V}_i \sim \mathcal{CN}\left(0, \sigma_n^2 Q\right). \tag{67}$$

We obtain

$$\widetilde{C}_i + \Re(\widetilde{V}_i) \sim \mathcal{N}\left(\rho \sum_{q=0}^{Q-1} \mu(f_q), \rho^2 \sum_{q=0}^{Q-1} \Phi(f_q) + \frac{\sigma_n^2}{2}Q\right) \tag{68}$$

$$\Im(\widetilde{V}_i) \sim \mathcal{N}\left(0, \frac{\sigma_n^2}{2}Q\right). \tag{69}$$

We stack the real and the imaginary parts of the $R_{l,i}$ in (66) for $i = 1, \cdots M$, to create the $2M \times 1$ vector

$$\mathbf{z}_l = \left[[\Re(\mathbf{r}_l)]^T, \ [\Im(\mathbf{r}_l)]^T\right]^T. \tag{70}$$

From the results in Appendix II, the test statistic for the TR-MIMO detector is

$$\ell_{\mathrm{TR}}(\mathbf{r}_l) = \frac{\sum_{q=0}^{Q-1} \Phi(f_q)}{\sigma_n^2 Q} \, ||\Re(\mathbf{r}_l)||^2 + \left(\sum_{q=0}^{Q-1} \mu(f_q)\right) \Re(\mathbf{r}_l)^T \mathbf{1}_N. \tag{71}$$

The detector uses (71) to calculate the decision threshold under the null hypothesis $\mathbb{H}_0$.

C. About the Output of Matched Filters

In Step 3 of Section III-A, the ith entry $X_{l,i}$ of $\mathbf{x}_l(f_q)$ defined in (37), is matched with the originally transmitted signal at the ith antenna, i.e., $S_i(f_q)$ defined in (33). One can certainly match $X_{l,i}$ with other signals $S_m(f_q)$, $m \neq i$ to generate a total of $M(M-1)$ outputs. Excluding the additive noise terms, these outputs are

$$\widetilde{C}_{im} \triangleq \sum_{q=0}^{Q-1} C_i(f_q) S_m(f_q). \tag{72}$$

Since $h_{ij}(f_q)$ and $\bar{h}_{ij}(f_q), \forall i,j$ are random variables, we take the expectation of $\widetilde{C}_{im}$

$$E\{\widetilde{C}_{im}\} = \sum_{q=0}^{Q-1}\sum_{n=1}^{N} E\left\{k\bar{h}_{ni}(f_q)h^*_{nm}(f_q)\right\}|S_m(f_q)|^2 + \sum_{q=0}^{Q-1}\sum_{j\neq n}^{N} E\left\{k\sum_{n=1}^{N}\bar{h}_{ni}(f_q)h^*_{nj}(f_q)\right\} \times S^*_j(f_q)S_m(f_q) \quad (73)$$

$$= \rho\cdot\sum_{q=0}^{Q-1}\sum_{n=1}^{N} E\left\{kh_{ni}(f_q)h^*_{nm}(f_q)\right\}|S_m(f_q)|^2 + \sum_{q=0}^{Q-1}\sum_{n=1}^{N} E\left\{k\gamma_{ni}(f_q)h^*_{nm}(f_q)\right\}|S_m(f_q)|^2 + \sum_{q=0}^{Q-1}\sum_{j\neq n}^{N} E\left\{k\sum_{n=1}^{N}\bar{h}_{ni}(f_q)h^*_{nj}(f_q)\right\} \times S^*_j(f_q)S_m(f_q) \quad (74)$$

$$= \rho\cdot\sum_{q=0}^{Q-1}\sum_{n=1}^{N} E\left\{k|h_{ni}(f_q)|^2\right\}\delta(i-m)|S_m(f_q)|^2 + \rho\cdot\sum_{q=0}^{Q-1}\sum_{j\neq n}^{N}\sum_{n=1}^{N} E\left\{k|h_{ni}(f_q)|^2\right\} \times \delta(i-j)S^*_j(f_q)S_m(f_q) \quad (75)$$

$$= \rho\cdot\sum_{q=0}^{Q-1} E\left\{k|h_{ni}(f_q)|^2\right\} \times S^*_i(f_q)S_m(f_q),\ \ i\neq m. \quad (76)$$

Hence

$$E\{\widetilde{C}_{im}\} = \rho\cdot E\{k\}\cdot\sum_{q=0}^{Q-1}\sigma_s^2(f_q)\cdot S^*_i(f_q)S_m(f_q),\ \ i\neq m. \quad (77)$$

We argue now that (77) is a complex number with small magnitude compared with (53). This is the result of the orthogonality between $S_i(f_q)$ and $S_m(f_q), i\neq m$, chosen in Section II-C. In particular, if the term $E\{k|h_{ni}(f_q)|^2\} = k\sigma_s^2$, a constant value independent of frequency, (77) becomes zero. Therefore, we do not consider these $M(M-1)$ outputs from the matched filters.

D. Statistical MIMO Detector

The statistical MIMO (S-MIMO) radar discussed in the literature is designed for narrowband radar [10], [20]. We extend this narrowband signal model, (1) and (2), to wideband. One of the key processing steps in S-MIMO is to extract the complex gains of a total of $M\times N$ channels. When using wideband orthogonal waveform signaling, we implement the orthogonal phase coding given in (24), which corresponds to the same waveforms that we used for TR-MIMO. Similar to the development of the TR-MIMO detector, we assume a homogeneous clutter model. In this case, compared with (38), the received signal for S-MIMO is

$$\mathbf{z}_l(f_q) = \overline{\mathbf{H}}^T(f_q)\mathbf{s}_B(f_q) + \mathbf{v}_l(f_q) \quad (78)$$

where

$$\mathbf{s}_B = \sqrt{\frac{M}{N}}\left[S_1(f_q),\cdots,S_N(f_q)\right]^T \quad (79)$$

$$\mathbf{z}_l(f_q) = \left[Z_{l,1}(f_q),\cdots,Z_{l,M}(f_q)\right]^T \quad (80)$$

$$Z_{l,m}(f_q) = \sqrt{\frac{M}{N}}\sum_{i=1}^{N} h_{mi}(f_q)S_i(f_q) + V_{l,m}(f_q). \quad (81)$$

It is straightforward to derive that

$$Z_{l,m}(f_q) \sim \mathcal{CN}\left(0, M\sigma_s^2(f_q)+\sigma_n^2\right). \quad (82)$$

By the statistical MIMO processing scheme in [20], matched-filtering the received signals with the orthogonal waveforms $\{S_n(f_q), n=1,\cdots,N\}$ given in (24) yields

$$U_{l,mn} = \sum_{q=0}^{Q-1} Z_{l,m}(f_q)\sqrt{\frac{M}{N}}S^*_n(f_q) = \widetilde{h}_{mn} + \widetilde{V}_{l,mn} \quad (83)$$

where

$$\widetilde{h}_{mn} = \frac{M}{N}\sum_{q=0}^{Q-1}\sum_{i=1}^{N} h_{mi}(f_q)S_i(f_q)S^*_n(f_q), \quad (84)$$

$$\widetilde{V}_{l,mn} = \sum_{q=0}^{Q-1} V_{l,m}(f_q)\sqrt{\frac{M}{N}}S^*_n(f_q). \quad (85)$$

We group the quantities $U_{l,mn}$, $\widetilde{h}_{l,mn}$, and $\widetilde{V}_{l,mn}$ into $MN\times 1$ vectors

$$\mathbf{u}_l = [U_{l,11}, U_{l,12},\cdots,U_{l,MN}]^T \quad (86)$$

$$\widetilde{\mathbf{h}}_l = [\widetilde{h}_{l,11}, \widetilde{h}_{l,12},\cdots,\widetilde{h}_{l,MN}]^T \quad (87)$$

$$\widetilde{\mathbf{v}}_l = [\widetilde{V}_{l,11}, \widetilde{V}_{l,12},\cdots,\widetilde{V}_{l,MN}]^T. \quad (88)$$

Thus, the binary hypothesis test for S-MIMO is given by

$$\begin{aligned}\mathbb{H}_1:\ \mathbf{u}_l &= \widetilde{\mathbf{h}}_l + \widetilde{\mathbf{v}}_l\\ \mathbb{H}_0:\ \mathbf{u}_l &= \widetilde{\mathbf{v}}_l.\end{aligned} \quad (89)$$

We use the following test statistic for MIMO radar [20]:

$$\ell_{\mathrm{S-MIMO}}(\mathbf{u}_l) = \|\mathbf{u}_l\|^2 = \sum_{m=1}^{M}\sum_{i=1}^{N}|U_{l,mn}|^2 \quad (90)$$

This detector computes the threshold under the null hypothesis $\mathbb{H}_0$.

V. Performance Analysis

In this section, we derive the test statistic for time reversal MIMO (TR-MIMO) in (71) and statistical MIMO (S-MIMO) in (90), respectively. To derive the detectors and to analyze their performance, we derive the probability density functions of the test statistics under $\mathbb{H}_1$ and $\mathbb{H}_0$, respectively. The performance analysis under the homogeneous clutter assumption provides insight on the tradeoffs between the number of antennas, the number of frequency samples of the proposed wideband MIMO radar detectors. We rely on numerical simulations to study channel decorrelation.

A. TR-MIMO

Under $\mathbb{H}_1$ and based on (68), we know that $\widetilde{C}_i+\Re(\widetilde{V}_i)$ are independent and identically distributed normal random variables for $i=1,\cdots,M$. Therefore, from (71), we obtain

$$\begin{aligned}\ell_{\mathrm{TR};\mathbb{H}_1} &= \frac{\sum_{q=0}^{Q-1}\Phi(f_q)}{\sigma_n^2 Q}\sum_{i=1}^{M}\left(\widetilde{C}_i+\Re(\widetilde{V}_i)\right)^2 \\ &\quad+\left(\sum_{q=0}^{Q-1}\mu(f_q)\right)\sum_{i=1}^{M}\left(\widetilde{C}_i+\Re(\widetilde{V}_i)\right) \qquad (91)\\ &\sim \frac{\sum_{q=0}^{Q-1}\Phi(f_q)}{\sigma_n^2 Q}\left(\rho^2\sum_{q=0}^{Q-1}\Phi(f_q)+\frac{\sigma_n^2}{2}Q\right)\chi^2_M(\gamma^2) \\ &\quad+\left(\sum_{q=0}^{Q-1}\mu(f_q)\right)\mathcal{N}\left(M\rho\sum_{1=0}^{Q-1}\mu(f_q),\right. \\ &\qquad\left. M\rho^2\sum_{q=0}^{Q-1}\Phi(f_q)+M\frac{\sigma_n^2}{2}Q\right) \qquad (92)\end{aligned}$$

where $\chi^2_M(\gamma^2)$ denotes the non-central Chi-squared distributed random variable with M degrees of freedom and the non-centrality parameter

$$\gamma^2 = M\frac{\rho^2\left(\sum_{q=0}^{Q-1}\mu(f_q)\right)^2}{\rho^2\sum_{q=0}^{Q-1}\Phi(f_q)+\frac{\sigma_n^2}{2}Q}. \qquad (93)$$

Under $\mathbb{H}_0$

$$\begin{aligned}\ell_{\mathrm{TR};\mathbb{H}_0} &= \frac{\sum_{q=0}^{Q-1}\Phi(f_q)}{\sigma_n^2 Q}\sum_{i=1}^{M}\left(\Re(\widetilde{V}_i)\right)^2 \\ &\quad+\left(\sum_{q=0}^{Q-1}\mu(f_q)\right)\sum_{i=1}^{M}\left(\Re(\widetilde{V}_i)\right) \qquad (94)\\ &\sim \frac{\sum_{q=0}^{Q-1}\Phi(f_q)}{\sigma_n^2 Q}\left(\frac{\sigma_n^2}{2}Q\right)\chi^2_M(0) \\ &\quad+\left(\sum_{q=0}^{Q-1}\mu(f_q)\right)\mathcal{N}\left(0,M\frac{\sigma_n^2}{2}Q\right) \\ &\sim \left(\frac{1}{2}\sum_{q=0}^{Q-1}\Phi(f_q)\right)\chi^2_M(0) \\ &\quad+\left(\sum_{q=0}^{Q-1}\mu(f_q)\right)\mathcal{N}\left(0,M\frac{\sigma_n^2}{2}Q\right) \qquad (95)\end{aligned}$$

where $\chi^2_M(0)$ is a central Chi-squared random variable with M degrees of freedom. Both (92) and (95) provide a simple description of the test statistic for the TR-MIMO detector under each hypothesis. To obtain the detection probability and the decision threshold from (92) and (95), we derive in Appendix III the probability density functions $f_{\ell_1,\mathrm{TR}}(\ell_1)$ under $\mathbb{H}_1$ and $f_{\ell_0,\mathrm{TR}}(\ell_0)$ under $\mathbb{H}_0$, respectively. Given the density function $f_{\ell_0,\mathrm{TR}}(\ell_0)$ and a chosen false alarm rate P_{FA}, we can numerically calculate the threshold η_{TR} by solving

$$P_{\mathrm{FA}} \triangleq P_r(\ell_{\mathrm{TR}}>\eta|\mathbb{H}_0)=\int_{\eta_{\mathrm{TR}}}^{\infty} f_{\ell_0,\mathrm{TR}}(\ell_0)d\ell_0 \qquad (96)$$

Readers can refer to Appendix III for a detailed discussion on how the threshold η_{TR} is computed. Next, we can compute the detection probability

$$P_{\mathrm{D}} \triangleq P_r(\ell_{\mathrm{TR}}>\eta|\mathbb{H}_1)=\int_{\eta_{\mathrm{TR}}}^{\infty} f_{\ell_1,\mathrm{TR}}(\ell_1)d\ell_1. \qquad (97)$$

Under simplifying conditions, for example, the radar signal model given in [35] and [36], one can develop closed form expressions for P_{D} and P_{FA}. In our case, the time reversal radar signal model in (66) becomes, approximately, a nonzero mean, real Gaussian signal immersed in zero-mean complex Gaussian noise. The mathematical tractability of closed form expressions for P_{D} and P_{FA} becomes difficult. One can resort to importance sampling to efficiently calculate these quantities (see, e.g., [37], [38]).

B. Statistical MIMO Detector

From (90), under the null hypothesis $\mathbb{H}_0$, $V_{l,m}(f_q)\sim\mathcal{CN}(0,\sigma_n^2)$. For a fixed m

$$\begin{aligned}&\sum_{n=1}^{N}\left|\sum_{q=0}^{Q-1}V_{l,m}(f_q)\sqrt{\frac{M}{N}}S_n^*(f_q)\right|^2 \\ &\quad=\sum_{n=1}^{N}\mathbf{v}_{l,m}^H\mathbf{s}_n\mathbf{s}_n^H\mathbf{v}_{l,m} \qquad (98)\\ &\quad=\frac{M}{N}\mathbf{v}_{l,m}^H\sum_{n=1}^{N}\left(\mathbf{s}_n\mathbf{s}_n^H\right)\mathbf{v}_{l,m} \qquad (99)\end{aligned}$$

where

$$\mathbf{v}_{l,m}=[V_{l,m}(f_0),\cdots,V_{l,m}(f_{Q-1})]^T \qquad (100)$$

$$\mathbf{s}_n=[S_n(f_0),\cdots,S_n(f_{Q-1})]^T. \qquad (101)$$

Furthermore, we define

$$\mathbf{\Pi}\triangleq\sum_{n=1}^{N}\left(\mathbf{s}_n\mathbf{s}_n^H\right) \qquad (102)$$

where the (q_1,q_2)th entry of $\mathbf{\Pi}$ is given by

$$\begin{aligned}&\sum_{n=1}^{N}e^{j2\pi\frac{n}{Q}(q_1-q_2)} \\ &\quad=e^{j2\pi\frac{q_1-q_2}{Q}}\frac{1-e^{j2\pi\frac{q_1-q_2}{Q}N}}{1-e^{j2\pi\frac{q_1-q_2}{Q}}} \qquad (103)\end{aligned}$$

$$= e^{j\pi\frac{q_1-q_2}{Q}(N+1)}\frac{\sin\left(\pi(q_1-q_2)N/Q\right)}{\sin\left(\pi(q_1-q_2)/Q\right)} \quad (104)$$

$$= e^{j\pi\frac{q_1-q_2}{Q}(N+1)}\frac{\operatorname{sinc}\left((q_1-q_2)N/Q\right)}{\operatorname{sinc}\left((q_1-q_2)/Q\right)}N. \quad (105)$$

We further define the following two matrices $\mathbf{\Lambda}$ and $\mathbf{\Upsilon}$

$$[\mathbf{\Lambda}]_{q_1,q_2} \triangleq \frac{\operatorname{sinc}\left((q_1-q_2)N/Q\right)}{\operatorname{sinc}\left((q_1-q_2)/Q\right)}N \quad (106)$$

$$\mathbf{\Upsilon} \triangleq \operatorname{diag}\left\{\left[1, e^{j\frac{\pi}{Q}(N+1)}, \cdots, e^{j\frac{\pi}{Q}(N+1)(Q-1)}\right]\right\}. \quad (107)$$

We immediately recognize that

$$\mathbf{\Pi} = \mathbf{\Upsilon}^H\mathbf{\Lambda}\mathbf{\Upsilon}. \quad (108)$$

Hence, (99) can be rewritten as

$$\sum_{n=1}^{N}\left|\sum_{q=0}^{Q-1}V_{l,m}(f_q)\sqrt{\frac{M}{N}}S_n^*(f_q)\right|^2 = \frac{M}{N}(\mathbf{\Upsilon}\mathbf{v}_{l,m})^H\mathbf{\Lambda}(\mathbf{\Upsilon}\mathbf{v}_{l,m}). \quad (109)$$

Note that the matrix $\mathbf{\Lambda}$ has N identical singular values

$$\lambda_n = Q, \quad n = 1, \cdots, N. \quad (110)$$

Each entry of the vector $\mathbf{\Upsilon}\mathbf{v}_{l,m}$ is a complex Gaussian random variable with zero mean and variance σ_n^2. Hence, (109) can be written as a quadratic form

$$\sum_{n=1}^{N}\left|\sum_{q=0}^{Q-1}V_{l,m}(f_q)\sqrt{\frac{M}{N}}S_n^*(f_q)\right|^2 = \frac{M}{N}\sum_{n=1}^{N}\lambda_n|X_n|^2 \sim \frac{M}{N}Q\frac{\sigma_n^2}{2}\chi_{2N}^2 \quad (111)$$

where $X_n \sim \mathcal{CN}(0,\sigma_n^2)$. Since $\{V_{l,m}(f_q), m = 1, \cdots, M\}$ are independent, complex random variables, we have

$$l_0 = \sum_{m=1}^{M}\sum_{n=1}^{N}\left|\sum_{q=0}^{Q-1}V_{l,m}(f_q)\sqrt{\frac{M}{N}}S_n^*(f_q)\right|^2 \sim \frac{M}{N}Q\frac{\sigma_n^2}{2}\chi_{2MN}^2. \quad (112)$$

Under the alternative hypothesis $\mathbb{H}_1$, for a fixed m

$$\sum_{q=0}^{Q-1}\sum_{j=1}^{N}h_{mj}(f_q)S_j(f_q)S_n^*(f_q) \sim \mathcal{CN}\left(0, N\sum_{q=0}^{Q-1}\sigma_s^2(f_q)\right). \quad (113)$$

Hence,

$$l_1 = \sum_{m=1}^{M}\sum_{n=1}^{N}\left|\sum_{q=0}^{Q-1}\left(\frac{M}{N}\sum_{j=1}^{N}h_{mj}(f_q)S_j(f_q) + V_{l,m}(f_q)\right)S_n^*(f_q)\right|^2 \sim \frac{\left(\frac{M}{N}\right)^2 N\sum_{q=0}^{Q-1}\sigma_s^2(f_q) + \frac{M}{N}Q\sigma_n^2}{2}\chi_{2MN}^2. \quad (114)$$

The binary hypothesis test (89) for S-MIMO is given by

$$\ell_{\mathrm{S}} = \|\mathbf{u}_l\|^2 \sim \begin{cases}\left(\frac{M^2}{N}\sum_{q=0}^{Q-1}\frac{\sigma_s^2(f_q)}{2} + \frac{M}{N}Q\frac{\sigma_n^2}{2}\right)\chi_{2MN}^2 & \mathbb{H}_1\\ \frac{M}{N}Q\frac{\sigma_n^2}{2}\chi_{2MN}^2 & \mathbb{H}_0\end{cases}. \quad (115)$$

The detection probability is given by

$$\begin{aligned}P_{\mathrm{D}}^{\mathrm{S}} &= P_r(\ell_{\mathrm{S}} > \eta_{\mathrm{S}}|\mathbb{H}_1)\\ &= P_r\left(\left(\frac{M^2}{N}\sum_{q=0}^{Q-1}\frac{\sigma_s^2(f_q)}{2} + \frac{M}{N}Q\frac{\sigma_n^2}{2}\right)\chi_{2MN}^2 > \eta_{\mathrm{S}}\right)\\ &= 1 - \psi_{\chi^2_{(2MN,0)}}\left(\frac{\eta_{\mathrm{S}}}{\left(\frac{M^2}{N}\sum_{q=0}^{Q-1}\frac{\sigma_s^2(f_q)}{2} + \frac{M}{N}Q\frac{\sigma_n^2}{2}\right)}\right)\\ &= 1 - \psi_{\chi^2_{(2MN,0)}}\left(\frac{Q\sigma_n^2\psi^{-1}_{\chi^2_{(2MN,0)}}(1-P_{\mathrm{FA}})}{M\sum_{q=0}^{Q-1}\sigma_s^2(f_q) + Q\sigma_n^2}\right). \quad (116)\end{aligned}$$

C. Discussion—Nominal Performance

Although the probability of detection is the most useful metric for comparing performance between different test statistics, other performance measures can also provide insight and mathematically tractable approaches; for example, the nominal performance given in [39, (p. 329)] . Here, we use the following metric [20]

$$\psi \triangleq \frac{\left|E\{\ell|\mathbb{H}_1\} - E\{\ell|\mathbb{H}_0\}\right|^2}{\frac{1}{2}\left(\operatorname{Var}\{\ell|\mathbb{H}_1\} + \operatorname{Var}\{\ell|\mathbb{H}_0\}\right)} \quad (117)$$

where ℓ denotes a test statistic, and ψ represents the normalized J-divergence between $\mathbb{H}_1$ and $\mathbb{H}_0$ hypothesis. Equation (117) is a simple measure to illustrate the performance of the detector. To simplify the calculation, we assume that

$$\sigma_s^2(f_q) = \sigma_s^2 \quad (118)$$

is frequency independent. We further define $\alpha \triangleq (\sigma_s^2/\sigma_n^2)$. Thus, from (162) in Appendix IV, we obtain (119) shown at the bottom of the page. Similarly, we obtain the ψ value for the S-MIMO

$$\psi_{\mathrm{S}} = \frac{2M^3N\alpha^2}{1+(1+M\alpha)^2}. \quad (120)$$

To compare (119) and (120), we assume that $\alpha \gg 1$, which is in high signal-to-noise ratio (SNR). In this case, $\psi_{\mathrm{TR}} \approx (QM/2)$, while $\psi_{\mathrm{S}} \approx 2MN$. This implies that, with a few sparsely placed antennas, M and N can be small. If the channel multipath scattering is rich, i.e., $Q > 4N$, the TR-MIMO shows a higher performance than the S-MIMO. Fig. 2 depicts the nominal performance versus SNR for TR-MIMO and S-MIMO using $Q = 10$.

$$\psi_{\mathrm{TR}} = \frac{2M\alpha(1+\alpha NQ+NQ)^2}{2\alpha^2\left(\alpha+\frac{1}{2}\right)^2 + 4NQ\alpha^2\left(\alpha+\frac{1}{2}\right)Q^2N\left(\alpha+\frac{1}{2}\right)^2 + \frac{1}{2}\alpha(QN+1)} \quad (119)$$

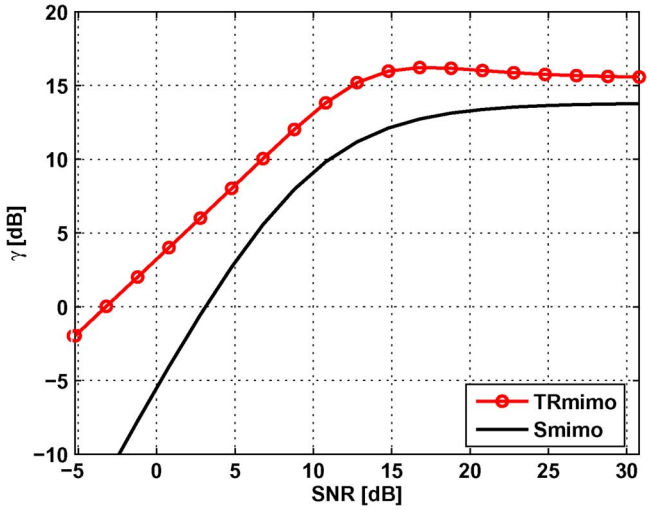

Fig. 2. Nominal performance versus SNR (α) for TR-MIMO and S-MIMO using $Q = 10$. $M = 2$ transmit antennas and $N = 3$ receive antennas.

VI. Numerical Simulations

In this section, we carry out numerical simulations to evaluate the performance of the proposed detectors. The simulation is carried out as follows: 1) generate random realizations of Q independent frequency samples for the $N \times M$ forward channel matrix $\mathbf{H}(f_q)$ and the $M \times N$ backward channel matrix $\overline{\mathbf{H}}^T(f_q)$; 2) generate orthogonal waveforms based on (24); 3) generate target signal independent additive noise and add the noise to the received radar returns; 4) calculate the test statistics and determine the decision threshold given the false alarm rate $P_{\rm FA}$; and 5) calculate the detection probability. The signal-to-noise ratio is defined as

$$\text{SNR} = \frac{\sum_{q=0}^{Q-1} \sigma_s^2(f_q)}{\sigma_n^2} \tag{121}$$

We choose $Q = 10$ frequencies, $M = 2$ transmit antennas, and $N = 3$ receive antennas for simulation purposes. We show in Fig. 3 the detection probability versus SNR for TR-MIMO versus S-MIMO under the false alarm rates of $P_{\rm FA} = [10^{-5}, 10^{-4}, 10^{-3}, 10^{-2}]$, respectively. The correlation factor $\rho = 1$ represents the ideal scenario. The analytical results are plotted using (97) for the TR-MIMO detector and (116) for the S-MIMO detector, respectively. The lines represent the analytical plots while the markers denote the Monte Carlo simulation results. Fig. 3(a)–(d) shows that the analytical results match the Monte Carlo simulation results quite well. The proposed TR-MIMO has about 14-dB gain over S-MIMO for the simulation setup $Q = 10$. There appears a small prediction bias (within a fraction of a dB) for the analytical ROC result compared with the Monte Carol simulation. This small prediction bias can be explained by the approximation we made in our analysis, for example, see (54). This equation argues that the unmatched phase terms are zero, which of course is not true in practice. This approximation yields slightly better performance and ROC curve than the Monte Carlo simulation shows, see Fig. 3. This prediction bias can be reduced by increasing the

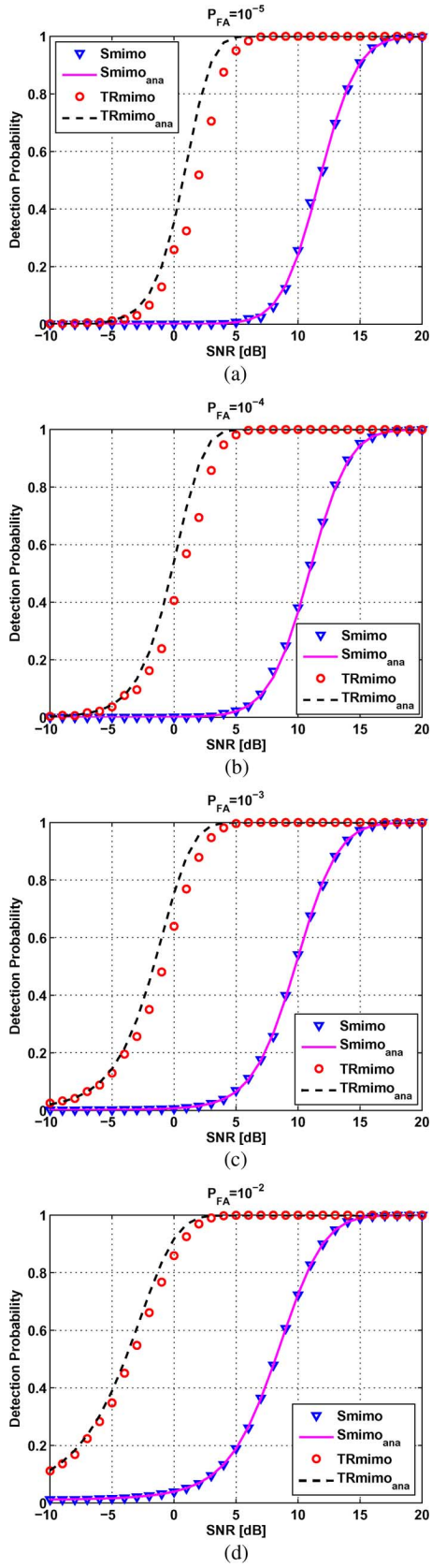

Fig. 3. Detection probability versus SNR for TR-MIMO and S-MIMO using $Q = 10$. The analytical results in the legend are marked with subscripts "ana" for the TR-MIMO detector and the S-MIMO detector. The simulation uses $M = 2$ transmit antennas and $N = 3$ receive antennas. The correlation between the forward channel and the backward channel is $\rho = 1$. The false alarm rates are: (a) $P_{\rm FA} = 10^{-5}$, (b) $P_{\rm FA} = 10^{-4}$, (c) $P_{\rm FA} = 10^{-3}$, and (d) $P_{\rm FA} = 10^{-2}$.

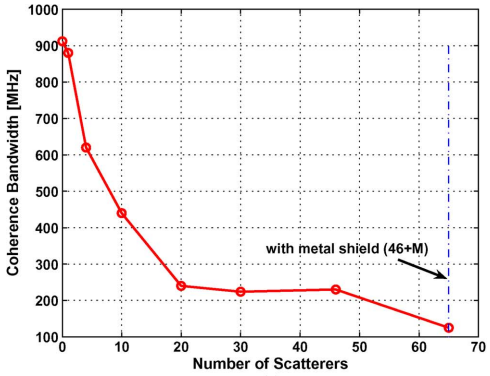

(a)

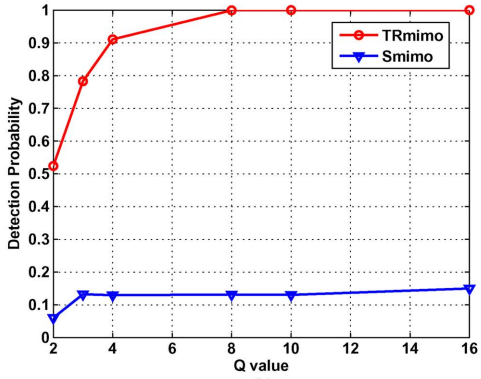

(b)

Fig. 4. (a) Average coherence bandwidth of scattering channels estimated from experimental electromagnetic data collected in lab, [9]. The average coherence bandwidth decreases from 912 to 120 MHz as the propagation medium becomes increasingly multipath rich. (b) Detection probability of TR-MIMO and S-MIMO by simulations assuming $Q = 2, 3, 4, 8, 10, 16$, respectively. $P_{\rm FA} = 10^{-4}$, $M = 2, N = 3$.

size N of the receiving antenna or the number of independent frequency bands Q.

The number of independent frequencies Q depends on the scattering properties of the channel and can be determined by experiments. In our case, the choice of Q is based on our experimental electromagnetic data collected in an increasingly rich scattering lab environment. The scattering environment is created using dielectric solid rods of 3.2-cm diameter, [9]. The details of the experiments are reported in [9]. The experiment synthesizes a wideband signal of 2 GHz (4–6 GHz) using stepped frequency signals generated by a vector network analyzer (VNA). The scattering environment is created by gradually increasing the number of dielectric rods in a 4×4 square feet wood platform. The wood platform has a total of 46 holes that can hold the dielectric rods vertically. First, the target response is measured for a copper target; then, we add one dielectric rod into the scene to create multipath. We keep adding dielectric rods until all the rods are filled in the holes. We then measure the coherence bandwidth B_c of the channel versus the number of dielectric rods. Fig. 4(a) shows that the coherence bandwidth decreases from $B_c = 912$ MHz to $B_c = 200$ MHz. To further enhance the channel scattering, we place a metal shield behind these 46 rods, which brings down

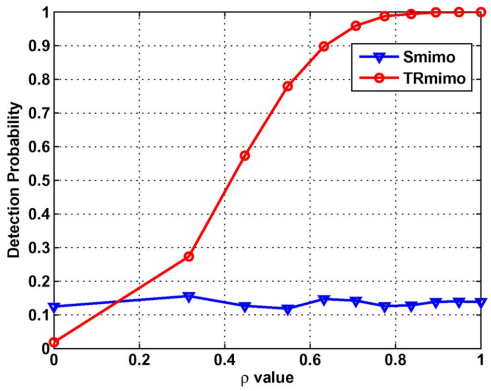

Fig. 5. Detection probability for TR-MIMO versus decorrelation factor ρ. The number of frequencies $Q = 10$. $M = 2, N = 3$. $P_{\rm FA} = 10^{-4}$.

the coherence bandwidth to 120 MHz. The-$B = 2$ GHz bandwidth corresponds to $Q = B/B_c = 2, 3, 4, 10, 16$, respectively. Using this sequence of Q values, we generate, by Monte Carlo simulations, the detection of probability versus Q in Fig. 4(b) for TR-MIMO and S-MIMO. We fix the average channel gain to noise ratio $\sum_{q=0}^{Q-1}/Q\sigma_n^2$ at -2 dB and change the Q value. Fig. 4(b) shows that the performance gain of TR-MIMO versus S-MIMO increases as the scattering becomes dense. This is because the TR-MIMO detector coherently process signals by adaptive time reversal transmission while the S-MIMO detector non-coherently add up signals from different frequencies.

To study the de-correlation between the forward channel and the backward channel in time reversal, we vary the correlation factor ρ in the range of 0 and 1. Fig. 5 depicts the detection probability of TR-MIMO and S-MIMO when the decorrelation factor ρ decreases from 1 to 0. The performance of TR-MIMO is robust against channel decorrelation.

VII. Conclusion

This paper develops the time reversal MIMO radar detector and provides an analytical expression for the probability distribution of TR-MIMO. The TR-MIMO exploits the spatial diversity arising from the multipath and adjusts the waveforms to the scattering properties of the medium by using time reversal. The paper presents a model for TR-MIMO that accounts for possible decorrelation between the forward channel and the backward channel and derives the test statistic, threshold, and probability of detection for the TR-MIMO Neyman–Pearson detector. The algorithm we develop is robust in rich multipath environments and shows a significant gain over the statistical MIMO detector.

Appendix I
Energy Normalization Scalar $\overline{k}$

The scalar k in (41) is a random variable because it depends on the channel matrix $\mathbf{H}(f_q)$ whose elements are random. In the development of the statistics for TR-MIMO, we wish to characterize the mean of this random variable as $\overline{k} = E(k)$, where

$$k^2 = \frac{MQE_s}{\sum_q \|\mathbf{H}(f_q)\mathbf{s}_A(f_q)\|^2} \tag{122}$$

where $E_s = (1/Q)\sum_{q=0}^{Q-1}|S(f_q)|^2$. Let the vector $\mathbf{p}(f_q) = [p_1(f_q),\cdots,p_N(f_q)]^T \triangleq \mathbf{H}(f_q)\mathbf{s}_A(f_q)$, where

$$p_n(f_q) = \sum_{j=1}^{M} S_j(f_q)h_{nj}(f_q) \sim \mathcal{CN}\left(0, M\sigma_s^2(f_q)\right) \quad (123)$$

where $h_{ij}(f_q) \sim \mathcal{CN}(0,\sigma_s^2(f_q))$, $|h_{ij}(f_q)|^2 \sim (\sigma_s^2(f_q)/2)\chi_2^2$, and we assume for simplicity $S(f_q) = 1$. It is straightforward to see that

$$\|\mathbf{p}(f_q)\|^2 = \sum_{n=1}^{N}|p_n(f_q)|^2 \sim \frac{M\sigma_s^2(f_q)}{2}\chi_{2N}^2. \quad (124)$$

Hence, using[40, Theorem 3.1], we obtain that the following weighted sum of independent Chi-squared random variables is

$$\sum_{q=0}^{Q-1}\|\mathbf{p}(f_q)\|^2 \sim g\chi_h^2 \quad (125)$$

where

$$g = \frac{M}{2}\frac{\sum_{q=0}^{Q-1}\sigma_s^4(f_q)}{\sum_{q=0}^{Q-1}\sigma_s^2(f_q)} \quad (126)$$

$$h = 2N\frac{\left(\sum_{q=0}^{Q-1}\sigma_s^2(f_q)\right)^2}{\sum_{q=0}^{Q-1}\sigma_s^4(f_q)}. \quad (127)$$

Hence, we obtain

$$k^2 = \frac{MQE_s}{\sum_{q=1}^{Q}\|\mathbf{p}(f_q)\|^2} \sim \frac{MQE_s}{g\chi_h^2}. \quad (128)$$

Hence, k^2 is distributed as a scaled inverse-chi-squared random variable. It is well known that, for $X \sim \chi_h^2(0)$, $Y = 1/X$ has the mean $E(Y) = 1/(h-2)$, $\forall h > 2$, and $\mathrm{Var}(Y) = 2/(h-2)^2(h-4)$, $\forall h > 4$. Hence, we obtain the mean of k^2 as follows:

$$E(k^2) = \frac{QE_s}{N\sum_{q=0}^{Q-1}\sigma_s^2(f_q) - \frac{\sum_{q=0}^{Q-1}\sigma_s^4(f_q)}{\sum_{q=0}^{Q-1}\sigma_s^2(f_q)}}. \quad (129)$$

In probability theory and statistics, the coefficient of variation (CV) is a normalized measure of the dispersion of a probability distribution. It is defined as the ratio of the standard deviation to the mean as

$$c_v \triangleq \frac{\sqrt{\mathrm{Var}(Y)}}{E(Y)} \quad (130)$$

$$= \sqrt{\frac{2}{h-4}} \quad (131)$$

$$= \sqrt{\frac{1}{N\frac{\left(\sum_q \sigma_s^2(f_q)\right)^2}{\sum_q \sigma_s^4(f_q)} - 2}}. \quad (132)$$

By the Cauchy–Schwartz inequality

$$\frac{\left(\sum_{q=0}^{Q-1}\sigma_s^2(f_q)\right)^2}{\sum_{q=0}^{Q-1}\sigma_s^4(f_q)} \geq 1.$$

Hence, for $N > 2$, we obtain

$$c_v \leq \sqrt{\frac{1}{N-2}} < 1 \quad (133)$$

which implies that k^2 has a low variance. This result implies that the variance of k^2 will be a very small number when the number of frequencies Q and the number of antennas are large. Hence, it suffices to say that k is approximately a constant.

Appendix II
Derivation of the TR-MIMO Detector

By (70), the probability density function of $\mathbf{z}_l$ under $\mathbb{H}_1$ is

$$f(\mathbf{z}_l|\mathbb{H}_1) = \frac{1}{(\sqrt{2\pi})^{2M}}\left(\det|\mathbf{\Sigma}_1|\right)^{-\frac{1}{2}} e^{-\frac{1}{2}(\mathbf{z}_l-\boldsymbol{\mu})^T\mathbf{\Sigma}_1^{-1}(\mathbf{z}_l-\boldsymbol{\mu})} \quad (134)$$

where

$$\boldsymbol{\mu} = \sum_{q=0}^{Q-1}\mu(f_q)\begin{bmatrix}\mathbf{1}_M\\ \mathbf{0}_M\end{bmatrix} \quad (135)$$

$$\mathbf{\Sigma}_1 = \begin{bmatrix}\left(\sum_{q=0}^{Q-1}\Phi(f_q) + \frac{\sigma_n^2}{2}Q\right)\mathbf{I}_M & \mathbf{0}_M\\ \mathbf{0}_M & \frac{\sigma_n^2}{2}Q\mathbf{I}_M\end{bmatrix}. \quad (136)$$

The symbols $\mathbf{1}_M, \mathbf{0}_M, \mathbf{I}_M$ stand for an $M\times 1$ vector that contains all 1s, an $M\times 1$ vector that contains all 0s, and an $M\times M$ identity matrix, respectively. Similarly, the probability density function of $\mathbf{z}_l$ under $\mathbb{H}_0$ is

$$f(\mathbf{z}_l|\mathbb{H}_0) = \frac{1}{(\sqrt{2\pi})^{2M}}\left(\det|\mathbf{\Sigma}_0|\right)^{-\frac{1}{2}} e^{-\frac{1}{2}\mathbf{z}_l^T\mathbf{\Sigma}_0^{-1}\mathbf{z}_l} \quad (137)$$

where

$$\mathbf{\Sigma}_0 = \frac{\sigma_n^2}{2}Q\mathbf{I}_{2M}. \quad (138)$$

The likelihood ratio test becomes

$$\begin{aligned}\ell_{\mathrm{TR}} &= \ln\frac{f(\mathbf{z}_l|\mathbb{H}_1)}{f(\mathbf{z}_l|\mathbb{H}_0)}\\ &= \ln f(\mathbf{z}_l|\mathbb{H}_1) - \ln f(\mathbf{z}_l|\mathbb{H}_0)\\ &= -\frac{1}{2}(\mathbf{z}_l-\boldsymbol{\mu})^T\mathbf{\Sigma}_1^{-1}(\mathbf{z}_l-\boldsymbol{\mu}) + \frac{1}{2}\mathbf{z}_l^T\mathbf{\Sigma}_0^{-1}\mathbf{z}_l. \quad (139)\end{aligned}$$

Using (70), and discarding the constant terms 1/2 in (139), we rewrite (139) as

$$\begin{aligned}\ell_{\mathrm{TR}} = &-\begin{pmatrix}\Re(\mathbf{r}_l) - \sum_{q=0}^{Q-1}\mu(f_q)\mathbf{1}_M\\ \Im(\mathbf{r}_l)\end{pmatrix}^T\\ &\times\mathbf{\Sigma}_1^{-1}\begin{pmatrix}\Re(\mathbf{r}_l) - \sum_{q=0}^{Q-1}\mu(f_q)\mathbf{1}_M\\ \Im(\mathbf{r}_l)\end{pmatrix}\\ &+\begin{pmatrix}\Re(\mathbf{r}_l)\\ \Im(\mathbf{r}_l)\end{pmatrix}^T\mathbf{\Sigma}_0^{-1}\begin{pmatrix}\Re(\mathbf{r}_l)\\ \Im(\mathbf{r}_l)\end{pmatrix} \quad (140)\end{aligned}$$

$$= -\frac{1}{\sum_{q=0}^{Q-1}\Phi(f_q)+\frac{\sigma_n^2}{2}Q}\left\|\Re(\mathbf{r}_l)-\sum_{q=0}^{Q-1}\mu(f_q)\mathbf{1}_M\right\|^2 - \frac{2}{\sigma_n^2 Q}\|\Im(\mathbf{r}_l)\|^2+\frac{2}{\sigma_n^2 Q}\|\Re(\mathbf{r}_l)\|^2 + \frac{2}{\sigma_n^2 Q}\|\Im(\mathbf{r}_l)\|^2 \quad (141)$$

$$= \frac{\sum_{q=0}^{Q-1}\Phi(f_q)}{\frac{\sigma_n^2 Q}{2}\left(\sum_{q=0}^{Q-1}\Phi(f_q)+\frac{\sigma_n^2}{2}Q\right)}\|\Re(\mathbf{r}_l)\|^2 + 2\frac{\sum_{q=0}^{Q-1}\mu(f_q)}{\sum_{q=0}^{Q-1}\Phi(f_q)+\frac{\sigma_n^2}{2}Q}\Re^T(\mathbf{r}_l)\mathbf{1}_M. \quad (142)$$

Discarding the common denominator in (142), we obtain (71).

APPENDIX III
DERIVATION OF DETECTION PROBABILITY AND THRESHOLD FOR TR-MIMO DETECTOR

We first rewrite (92) and (95) in the form of

$$\ell_i = A_i\chi_M^2(\gamma_i)+B_i\mathcal{N}(\mu_i,\Phi_i),\ \ i=0,1 \quad (143)$$

where we have the equation shown at the bottom of the page.

Note that for $z=x+y$, where x and y are independent random variables with probability density function $f_x(x)$ and $f_y(y)$, respectively, the probability density function of z is the convolution of $f_x(x)$ and $f_y(y)$, [34], i.e., $f_z(z)=\int_{-\infty}^{\infty}f_x(z-y)f_y(y)dy$. For $y=a\cdot x$, where a is a constant, the probability density function of y is given by $f_y(y)=(1/|a|)f_x(y/a)$.

Hence, under $\mathbb{H}_1$

$$f_{\ell_1,\mathrm{TR}}(\ell_1)=\int_0^{\infty}\frac{1}{A_1}f_{x_1}\left(\frac{x_1}{A_1}\right)\frac{1}{B_1}f_{y_1}\left(\frac{\ell_1-x_1}{B_1}\right)dx_1 \quad (145)$$

where the random variable $x_1\sim\chi_M^2(\gamma_1)$, and $y_1\sim\mathcal{N}(\mu_1,\Phi_1)$. Note that the probability density function of a non-central Chi-squared random variable x_1 is

$$f_{x_1}(x_1,M,\gamma_1)=\frac{1}{2}e^{-\frac{x_1+M}{2}}\left(\frac{x_1}{\gamma_1}\right)^{\frac{M}{4}-\frac{1}{2}}\times I_{\frac{M}{2}-1}(\sqrt{\gamma_1 x_1}),\quad x_1>0 \quad (146)$$

where $I_v(z)$ is a modified Bessel function of the first kind

$$I_v(z)\triangleq\left(\frac{z}{2}\right)^v\sum_{n=0}^{\infty}\frac{(z^2/4)^n}{n!\Gamma(v+n+1)}. \quad (147)$$

Further, notice that the Gaussian random variable y_1 has the probability density function

$$f_{y_1}(y_1)=\frac{1}{\sqrt{2\pi\Phi_1}}e^{-\frac{(y_1-\mu_1)^2}{2\Phi_1}} \quad (148)$$

which yields

$$f_{\ell_1,\mathrm{TR}}(\ell_1)=\frac{1}{A_1B_1}\int_0^{\infty}\frac{1}{2}e^{-\frac{x_1+M}{2}}\left(\frac{x_1}{\gamma_1}\right)^{\frac{M}{4}-\frac{1}{2}}I_{\frac{M}{2}-1}\times(\sqrt{\gamma_1 x_1})\frac{1}{\sqrt{2\pi\Phi_1}}e^{-\frac{\left(\frac{\ell_1-x_1}{B_1}-\mu_1\right)^2}{2\Phi_1}}dx_1. \quad (149)$$

Similarly, under $\mathbb{H}_0$, the probability density function

$$f_{\ell_0,\mathrm{TR}}(\ell_0)=\int_0^{\infty}\frac{1}{A_0}f_{x_0}\left(\frac{x_0}{A_0}\right)\frac{1}{B_0}f_{y_0}\left(\frac{\ell_0-x_0}{B_0}\right)dx_0 \quad (150)$$

where the random variable $x_0\sim\chi_M^2(0)$, and $y_0\sim\mathcal{N}(0,\Phi_0)$. Note that the probability density function of a central Chi-squared random variable x_0 is

$$f_{x_0}(x_0,M)=\frac{1}{2^{\frac{N}{2}}\Gamma\left(\frac{M}{2}\right)}x_0^{\frac{M}{2}-1}e^{-\frac{x_0}{2}},\quad x_0>0. \quad (151)$$

The Gaussian random variable y_0 has the probability density function

$$f_{y_0}(y_0)=\frac{1}{\sqrt{2\pi\Phi_0}}e^{-\frac{y_0^2}{2\Phi_0}} \quad (152)$$

which yields

$$f_{\ell_0,\mathrm{TR}}(\ell_0)=\frac{1}{A_0B_0}\int_0^{\infty}\frac{1}{2^{\frac{M}{2}}\Gamma\left(\frac{M}{2}\right)}\left(\frac{x_0}{A_0}\right)^{\frac{M}{2}-1}\times e^{-\frac{x_0}{2A_0}}\frac{1}{\sqrt{2\pi\Phi_0}}e^{-\frac{\left(\frac{\ell_0-x_0}{B_0}\right)^2}{2\Phi_0}}dx_0. \quad (153)$$

$$\begin{array}{ll} A_0=\frac{1}{2}\sum_{q=0}^{Q-1}\Phi(f_q), & A_1=\frac{\sum_{q=0}^{Q-1}\Phi(f_q)}{\sigma_n^2 Q}\left(\rho^2\sum_{q=0}^{Q-1}\Phi(f_q)+\frac{\sigma_n^2}{2}Q\right)\\ B_0=\sum_{q=0}^{Q-1}\mu(f_q), & B_1=\sum_{q=0}^{Q-1}\mu(f_q)\\ \mu_0=0, & \mu_1=M\rho\sum_{1=0}^{Q-1}\mu(f_q)\\ \Phi_0=M\frac{\sigma_n^2}{2}Q, & \Phi_1=M\rho^2\sum_{q=0}^{Q-1}\Phi(f_q)+M\frac{\sigma_n^2}{2}Q\\ \gamma_0=0, & \gamma_1=\gamma^2. \end{array} \quad (144)$$

Both (149) and (153) can be evaluated numerically.

To calculate the decision threshold η_{TR} and the detection probability $P_{\mathrm{D,TR}}$ in (97), we start from the probability density function (pdf) expressions in (145) and (150). We take the cumulative density function (cdf) as the integral along l from $-\infty$ to l_i, $i = 0, 1$

$$F_{l_i,\mathrm{TR}}(l_i) = \int_{-\infty}^{l_i} \int_{0}^{\infty} \frac{1}{A_i} f_{x_i}\left(\frac{x_i}{A_i}\right) \frac{1}{B_i} f_{y_i}\left(\frac{l - x_i}{B_i}\right) dx_i dl. \tag{154}$$

Shifting the order of integration allows us the expression

$$F_{l_i,\mathrm{TR}}(l_i) = \int_{0}^{\infty} \frac{1}{A_i} f_{x_i}\left(\frac{x_i}{A_i}\right) \int_{-\infty}^{l_i} \frac{1}{B_i} f_{y_i}\left(\frac{l - x_i}{B_i}\right) dl dx_i. \tag{155}$$

We note that the integral produces the cdf of the Gaussian random variable f_{y_i}. Thus,

$$F_{l_i,\mathrm{TR}}(l_i) = \int_{0}^{\infty} \frac{1}{A_i} f_{x_i}\left(\frac{x_i}{A_i}\right) F_{y_i}\left(\frac{l_i - x_i}{B_i}\right) dx_i. \tag{156}$$

This was solved with numerical integration. The inverse was accomplished via a simple search algorithm. The cdf is a nondecreasing function; therefore, comparison of the received cdf for some test point $F_{l_i,\mathrm{TR}}(l_t)$ against the desired cdf determines in which direction to increment the search term. For these tests, the stopping criteria was

$$|F_{l_i,\mathrm{TR}}(l_t) - \alpha| \leq 10^{-15}. \tag{157}$$

We use this inverse function to compute the threshold η_{TR} under the null hypothesis by calling

$$\eta_{\mathrm{TR}} = F^{-1}_{l_0,\mathrm{TR}}(P_{\mathrm{FA}}) \tag{158}$$

where $F^{-1}_{l_0,\mathrm{TR}}(P_{\mathrm{FA}})$ computes the numerical inverse described above. η_{TR} is then used to compute the detection probability

$$P_{\mathrm{D,TR}} = F_{l_1,\mathrm{TR}}(\eta_{\mathrm{TR}}) \tag{159}$$

Appendix IV
Calculation of the Nominal Performance for TR-MIMO and S-MIMO

Using the statistical properties of the Chi-squared distribution and normal distribution, from (143) and (144), we obtain

$$E\{\ell_{\mathrm{TR}}|\mathbb{H}_i\} = A_i(M + \gamma_i) + B_i\mu_i \tag{160}$$

$$\mathrm{Var}\{\ell_{\mathrm{TR}}|\mathbb{H}_i\} = A_i^2(2M + 4\gamma_i) + B_i^2\Phi_i. \tag{161}$$

A straightforward algebraic calculation yields the following:

$$\psi_{\mathrm{TR}} = \frac{\left(M(A_1 - A_0) + A_1\gamma_1 - A_0\gamma_0 + B_1\mu_1 - B_0\mu_0\right)^2}{M\left(A_1^2 + A_0^2\right) + 2\left(A_1^2\gamma_1 + A_0^2\gamma_0\right) + \left(B_1^2\Phi_1 + B_0^2\Phi_0\right)/2}. \tag{162}$$

References

[1] S. M. Garber, "High resolution sonar signals in a multipath environment," *IEEE Trans. Aerosp. Electron. Syst.*, vol. AES-2, no. 6, pp. 431–440, Nov. 1966.

[2] E. Daeipour, W. D. Blair, and Y. Bar-Shalom, "Bias compensation and tracking with monopulse radars in the presence of multipath," *IEEE Trans. Aerosp. Electron. Syst.*, vol. 33, no. 3, pp. 863–882, Jul. 1997.

[3] A. V. Mrstik and P. G. Smith, "Multipath limitations on low-angle radar tracking," *IEEE Trans. Aerosp. Electron. Syst.*, vol. AES-14, no. 1, pp. 85–102, Jan. 1978.

[4] D. A. Garren, A. C. Odom, M. K. Osborn, J. S. Goldstein, S. U. Pillai, and J. R. S. Guerci, "Full-polarization matched-illumination for target detection and identification," *IEEE Trans. Aerosp. Electron. Syst.*, vol. 38, no. 3, pp. 824–837, Jul. 2002.

[5] D. T. Gjessing, *Target Adaptive Matched-Illumination Radar: Principles and Applications*, ser. IEE Electromagnetic Waves Series. New York: Peter Peregrinus, 1986.

[6] M. Bell, "Information theory and RADAR waveform design," *IEEE Trans. Inf. Theory*, vol. 39, no. 5, pp. 1578–1597, Sep. 1993.

[7] J. M. F. Moura and Y. Jin, "Detection by time reversal: Single antenna," *IEEE Trans. Signal Process.*, vol. 55, no. 1, pp. 187–201, Jan. 2007.

[8] Y. Jin and J. M. F. Moura, "Time reversal detection using antenna arrays," *IEEE Trans. Signal Process.*, vol. 57, no. 4, pp. 1396–1414, Apr. 2009.

[9] Y. Jin, J. M. F. Moura, Y. Jiang, D. Stancil, and A. Cepni, "Time reversal detection in clutter: Additional experimental results," *IEEE Trans. Aerosp. Electron. Syst.*, to be published.

[10] E. Fishler, A. Haimovich, R. Blum, D. Chizhik, L. Cimini, and R. Valenzuela, "MIMO radar: An idea whose time has come," in *Proc. IEEE Radar Conf.*, April 2004, pp. 71–78, IEEE.

[11] G. J. Frazer, Y. I. Abramovich, and B. A. Johnson, "Spatially waveform diverse radar: Perspectives for high frequency OTHR," in *IEEE Radar Conf.*, Apr. 2007, IEEE.

[12] D. R. Fuhrmann and G. S. Antonio, "Transmit beamforming for MIMO radar systems using partial signal correlation," in *Proc. 38th Asilomar Conf. Signals, Syst., Comput.*, Pacific Grove, CA, Nov. 2004, vol. 1, pp. 295–299.

[13] F. Robey, S. Coutts, D. Weikle, J. McHarg, and K. Cuomo, "MIMO radar theory and experimental results," in *Proc. 38th Asilomar Conf. Signals, Syst., Comput.*, Pacific Grove, CA, Nov. 2004, vol. 1, pp. 300–304.

[14] K. Forsythe and D. Bliss, "Waveform correlation and optimization issues for MIMO radar," in *Proc. 39th Asilomar Conf. Signals, Syst., Comput.*, Pacific Grove, CA, Nov. 2005, pp. 1306–1310.

[15] J. Li, P. Stoica, and Y. Xie, "On probing signal design for MIMO radar," in *Proc. 40th Asilomar Conf. Signals, Syst., Comput.*, Pacific Grove, CA, Nov. 2006, vol. 1, pp. 31–35.

[16] S. L. Wilson and B. D. Carlson, "Radar detection in multipath," *IEE Proc.—Radar, Sonar Navig.*, vol. 146, no. 1, pp. 45–54, Feb. 1999.

[17] E. Bosse, R. Turner, and M. Lecours, "Tracking Swerling fluctuating targets at low altitude over the sea," *IEEE Trans. Aerosp. Electron. Syst.*, vol. 27, no. 5, pp. 806–822, Sep. 1991.

[18] Y. Jin and J. M. F. Moura, "TR-SAR: Time reversal target focusing in spotlight SAR," in *Proc. IEEE Int. Conf. Signal Process., ICASSP'07*, Honolulu, HI, Apr. 2007, vol. 2, pp. 957–960.

[19] J. M. F. Moura and Y. Jin, "Time reversal imaging by adaptive interference cancellation," *IEEE Trans. Signal Process.*, vol. 56, no. 1, pp. 1–15, Jan. 2008.

[20] E. Fishler, A. Haimovich, R. Blum, D. Chizhik, L. Cimini, and R. Valenzuela, "Spatial diversity in radars—Models and detection performance," *IEEE Trans. Signal Process.*, vol. 54, no. 3, pp. 823–838, Mar. 2006.

[21] G. S. Antonio and D. R. Fuhrmann, "Beampattern synthesis for wideband MIMO radar systems," in *1st IEEE Int. Workshop Comput. Adv. in Multi-Sensor Adaptive Process.*, San Antonio, TX, Dec. 2005, pp. 105–108.

[22] A. Isbimaru, *Wave Propagation and Scattering in Random Media*. Piscataway, NJ: IEEE Press, 1997.

[23] J. G. Proakis, *Digital Communications*, 3rd ed. New York: McGraw-Hill, 1995.

[24] B. Porat, *A Course in Digital Signal Processing*. New York: Wiley, 1999.

[25] D. R. Wehner, *High-Resolution Radar*. Boston, MA: Artech House, 1995.

[26] D. Liu, J. Krolik, and L. Carin, "Electromagnetic target detection in uncertain media: Time-reversal and minimum-variance algorithms," *IEEE Trans. Geosci. Remote Sens.*, vol. 45, no. 4, pp. 934–944, Apr. 2007.

[27] D. Liu, S. Vasudevan, J. Krolik, G. Bal, and L. Carin, "Electromagnetic time-reversal source localization in changing media: Experiment and analysis," *IEEE Trans. Antennas Propag.*, vol. 55, no. 2, pp. 344–354, Feb. 2007.

[28] R. McAulay and R. Yates, "Realization of the Gauss-in-Gauss detector using minimum-mean-squared-error filters," *IEEE Trans. Inf. Theory*, vol. 17, no. 2, pp. 207–209, Mar. 1971.
[29] L. Scharf, "Invariant Gauss-Gauss detection," *IEEE Trans. Inf. Theory*, vol. 19, no. 4, pp. 422–427, Jul. 1973.
[30] C. He and J. M. F. Moura, "Detection of multipath random signals by multiresolution subspace design," in *IEEE Int. Conf. Acoust., Speech, Signal Process. (ICASSP-97)*, Munich, Germany, Apr. 1997, vol. 5, pp. 3701–3704.
[31] R. Price, "Optimum detection of random signals in noise, with application to scatter-multipath communication—I," *IRE Trans. Inf. Theory*, vol. IT-2, no. 4, pp. 125–135, Dec. 1956.
[32] N. L. Johnson and S. Kotz, *Continuous Univariate Distributions*. New York: Wiley, 1970.
[33] P. Billingsley, *Convergence of Probability Measures*. New York: Wiley, 1968.
[34] A. Papoulis, *Probability, Random Variables, and Stochastic Processes*. New York: McGraw-Hill, 1991.
[35] R. S. Raghavan, H. F. Qiu, and D. J. McLaughlin, "CFAR detection in clutter with unknown correlation properties," *IEEE Trans. Aerosp. Electron. Syst.*, vol. 43, no. 2, pp. 647–657, Apr. 1995.
[36] E. J. Kelly, "An adaptive detection algorithm," *IEEE Trans. Aerosp. Electron. Syst.*, vol. AES-22, no. 22, pp. 115–127, Mar. 1986.
[37] R. Srinivasan and M. Rangaswamy, "Importance sampling for characterizing STAP detectors," *IEEE Trans. Aerosp. Electron. Syst.*, vol. 43, no. 1, pp. 273–285, Jan. 2007.
[38] R. L. Mitchell, "Importance sampling applied to simulation of false alarm statistics," *IEEE Trans. Aerosp. Electron. Syst.*, vol. AES-17, no. 1, pp. 15–24, Jan. 1981.
[39] H. L. VanTrees, *Detection, Estimation, and Modulation Theory: Part I*. New York: Wiley, 1968.
[40] G. E. P. Box, "Some theorems on quadratic forms applied in the study of analysis of variance problems, I. Effect of inequality of variance in th one-way classification," *Ann. Math. Statist.*, vol. 25, no. 2, pp. 290–302, Jun. 1954.

Yuanwei Jin (S'99–M'04–SM'08) received the B.S. and M.S. degrees from East China Normal University, Shanghai, China, in 1993 and 1996, respectively, and the Ph.D. degree in electrical and computer engineering from the University of California at Davis in 2003.

From 2003 to 2004, he was a Visiting Researcher with the University of California at Santa Cruz. From 2004 to 2008, he was a Post-Doctoral Research Fellow, then Project Scientist, with the Department of Electrical and Computer Engineering, Carnegie Mellon University, Pittsburgh, PA. Since August 2008, he has been an Assistant Professor with Department of Engineering and Aviation Sciences at the University of Maryland Eastern Shore, Princess Anne. His research interests are in the general area of statistical signal and image processing, with applications in radar/sonar, biomedical imaging, structure health monitoring, and wireless communications. He has published over 40 technical Journal and Conference papers.

Dr. Jin was a recipient of an Earle C. Anthony Fellowship from the University of California at Davis. He is affiliated with several IEEE societies, Sigma Xi, he American Society for Engineering Education (ASEE), and the American Association for Cancer Research (AACR).

José M. F. Moura (S'71–M'75–SM'90–F'94) received the engenheiro electrotécnico degree from the Instituto Superior Técnico (IST), Lisbon, Portugal, and the M.Sc., E.E., and D.Sc. degrees in electrical engineering and computer science from the Massachusetts Institute of Technology (MIT), Cambridge.

He is a Professor of Electrical and Computer Engineering and, by courtesy, of BioMedical Engineering, at Carnegie Mellon University (CMU), Pittsburgh, PA. He was on the faculty at IST, has held visiting faculty appointments at MIT, and was a Visiting Research Scholar at the University of Southern California, Los Angeles. He is a founding codirector of the Center for Sensed Critical Infrastructures Research (CenSCIR) and manages a large education and research program between Carnegie Mellon and Portugal (www.icti.cmu.edu). His research interests include statistical and algebraic signal processing, image, bioimaging, and video processing, and digital communications. He has published over 380 technical journal and conference papers, is the coeditor of two books, holds six patents, and has given numerous invited seminars at international conferences, U.S., European, and Japanese Universities, and industrial and government Laboratories.

Dr. Moura was the President (2008–09) of the IEEE Signal Processing Society (SPS) and vice-chair of the IEEE Publications Services and Products Board (2008). He was Editor in Chief for the IEEE TRANSACTIONS ON SIGNAL PROCESSING, interim Editor in Chief for the IEEE SIGNAL PROCESSING LETTERS, and was on the Editorial Board of several journals, including the IEEE PROCEEDINGS, the *IEEE Signal Processing Magazine*, and the ACM *Transactions on Sensor Networks*. He chaired the IEEE Transactions Committee that joins the Editors in Chief of the over 80 IEEE transactions and journals. He was on the steering and technical committees of numerous conferences. He is a Fellow of the American Association for the Advancement of Science (AAAS), and a corresponding member of the Academy of Sciences of Portugal (Section of Sciences). He was awarded the 2003 IEEE Signal Processing Society Meritorious Service Award and in 2000 the IEEE Millennium Medal. In 2007 he received the CMU's College of Engineering Outstanding Research Award and in 2008 the Philip L. Dowd Fellowship Award for contributions to engineering education. He is affiliated with several IEEE societies, Sigma Xi, AMS, IMS, and SIAM.

Nicholas O'Donoughue (S'03) received the B.S. degree in computer engineering from Villanova University, Villanova, PA, in 2006, and the M.S. degree in electrical and computer engineering from Carnegie Mellon University, Pittsburgh, PA, in 2008. He is currently pursuing the Ph.D. degree in electrical and computer engineering at Carnegie Mellon University.

His general research interests lie in the area of statistical signal processing, with applications in radar/sonar and communications, with a special interest in the technique of Time Reversal signal processing.

Mr. O'Donoughue is a recipient of the 2006 National Defense Science and Engineering Graduate (NDSEG) Fellowship, the 2006 Dean Robert D. Lynch Award from the Villanova University Engineering Alumni Society, and the 2006 Computer Engineering Outstanding Student Medallion from Villanova University. He has published more than a dozen technical journal and conference papers, including two that were chosen as *Best Student Paper*. He is a member of several IEEE societies, the Acoustical Society of America, Tau Beta Pi, and Eta Kappa Nu.